Physical model and sensitivity analysis of volume metering in centrifugal microfluidics

Auteur : Vanraes, Valentin
Promoteur(s) : Gilet, Tristan
Faculté : Faculté des Sciences appliquées
Diplôme : Master en ingénieur civil physicien, à finalité approfondie
Année académique : 2022-2023
URI/URL : http://hdl.handle.net/2268.2/18191

LIÈGE université
Sciences Appliquées

University of Liege
Faculty of Applied Sciences

Master Thesis realised to obtain the degree of Master of Science in Engineering Physics.

Physical model and sensitivity analysis of volume metering in centrifugal microfluidics.

Student:
Vanraes Valentin
Supervisor:
Gilet Tristan

Jury members:
Arnst Maartens
Straat Julien
Terrapon Vincent

Academic year 2022-2023

ABSTRACT

In the context of the Medicare project, precise micro-litre of liquid must be selected through a metering operation unit integrated into a centrifugal microfluidic chip. The experimenters have highlighted the dependency of the selected volume with respect to the shape of the liquid-air interface. As the experiments are expensive, numerical methods must be developed in order to study the sensitivity of the selected volume with respect to geometrical and physical parameters that must be identified.

A 3D model using the Surface Evolver program as well as a 2D analytical model have been developed in order to perform a sensitivity analysis on the selected volume with respect to the geometry of the chamber, the capillary length and the contact angle. By comparing the results of the two models with each other and with the experiments it has been proved that they both predict with accuracy the shape of the liquid-air interface and the volume in the chamber.

The results of the sensitivity analysis have demonstrated that there exists some proportionality between the volume and the geometrical and physical parameters of the experiments. In addition, it has been established that the volume is the most sensitive to the capillary number, and so to the centrifugal acceleration of the microfluidic chip, and to the depth of the metering chamber. Finally, the study of the impact of the height of the operation unit with respect to the contact angle has proven that several shapes of the interface can coexist for the same height. However, the range of height where this phenomenon could happen is of the order of a tenth of a millimetre.

ACKNOWLEDGEMENT

I would like to express my heartfelt gratitude to my supervisor, Tristan Gilet, for his unwavering support, guidance, and availability throughout the entire academic year. His insightful feedback and dedication have been invaluable in shaping this master thesis.

I extend my appreciation to Kenneth Brakke, the creator of the Surface Evolver program, for his generous advice and assistance. His insights into the program and his willingness to help have been instrumental in navigating its intricacies.

A special acknowledgement goes to my father for his patient assistance in making the Surface Evolver program compatible with my Mac. This technical expertise and his willingness to troubleshoot challenges have been instrumental in the successful execution of this research.

I would like to extend my sincere appreciation to my jury members Maartens Arnst, Julien Straat and Vincent Terrapon for graciously agreeing to evaluate and assess my master thesis.

I am deeply thankful to my family and friends, especially to Adrien, Hugo, Louis and Léa who have accompanied me throughout my years of study, for their unwavering support, encouragement, and understanding during this journey. Their belief in me has been a constant source of motivation.

CONTENTS

INTRODUCTION

Context and motivation

In order to immediately offer accurate and prompt diagnoses at the field level, at the patient's bedside, or at the scene of outbreaks, Point-Of-Care Tests (POCT) and Point-Of-Need Tests (PONT) have been established. These tests can guide medical professionals and decision-makers in swiftly taking the appropriate action. One way to do point-of-need tests is to use Lab-on-Chips (LoC) and microfluidic technologies. Several laboratory procedures have been automated and reduced in size to fit inside a small device [1].

Microfluidic devices work with small amounts of liquid and allow automation and high throughput screening [2]. They offer the potential to shorten turnaround times and, once fully designed, lower costs for analytical instruments, particularly in the fields of medicine, veterinary medicine, and environmental sciences [3]. More precisely, it consists in integrating one or several laboratory functions into a single chip, called a microfluidic chip.

In this context, the Medicare project aims at designing a device that uses Point-Of-Need (PON) microfluidics to measure antibiotic concentration and adjust dosage every hour (instead of every day). It is a Walloon Region project with ULiege (Center for Protein Engineering & microfluidics Lab), UCLouvain (Molecular Chemistry, Materials and Catalysis) and Unisensor (Liège Science Park). More specifically, this project takes advantage of a type of microfluidic technology called centrifugal microfluidic chip.

Centrifugal microfluidic chip, also known as Lab-on-a-Disc (LoD), is a platform that integrates multiple essential processes such as separation, mixing, reaction, and detection of nano-sized molecules within a single compact disk or DVD. Centrifugal microfluidic has one main advantage, it combines the benefits of both microfluidics and centrifugal forces in a single device. In concrete terms, the centrifugal, Coriolis, and Euler forces that are produced when the microfluidic disc rotates at various spinning rates can each be used to automate a variety of microfluidic device functions. Through the use of non-inertial valves and switches, fluids are dynamically manipulated in a highly parallel manner, enabling the efficient and precise perfor-

mance of lab-on-chip functionalities [4].

In order to obtain reproducible results, LoD must use precise volumes of liquids. Thus, these chips use special designs in order to select the precise volume, this is called volume metering [5]. In the case of the LoD used in the Medicare project, this operation unit consists in two chambers, called respectively metering and waste chambers. The liquid flows into the metering chamber from an inlet and once this metering chamber is filled, the excess of liquid flows into the waste chamber. After that, only the liquid staying in the metering chamber is used to perform the analysis. This is often coupled with a valve that opens when the process is finished, i.e. when the metering chamber is full. This system is depicted Fig. 1 and the full experimental system is shown in Fig. 2 and Fig. 3.

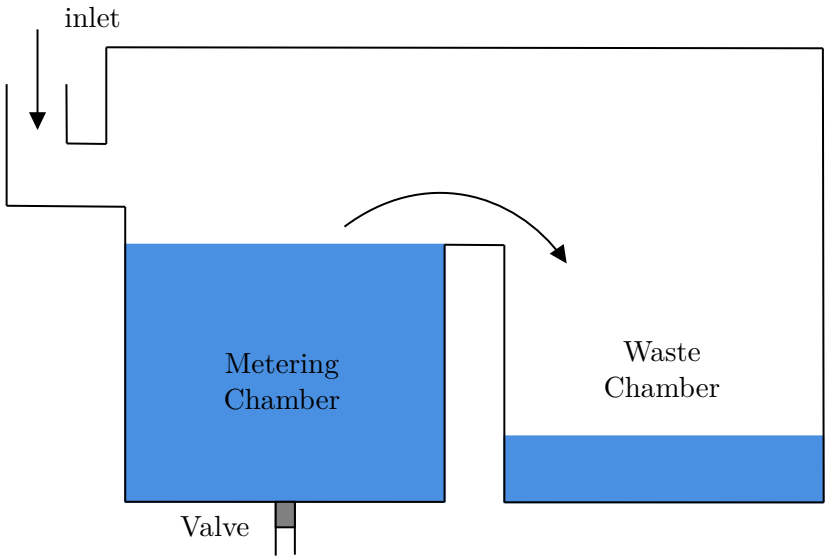

Figure 1: Representation of an operation unit for volume metering. Figure adapted from [5]

The main default of this operating unit is that the metering accuracy results from the balance between centrifugal forces and capillary forces. In fact, the microfluidics Lab noticed that this balance is significantly affected by the shape that the liquid interfaces may take when confined by the walls of the LoD. The results of experiments showed that equilibrium states may coexist, with interface shapes that are scarcely predictable and that can nevertheless interfere with the microfluidic operations. Results obtained in two experiments are depicted in Fig. 2 and Fig. 3, showing the shape of the interface just before the liquid flows in the waste chamber and shape just before the valve is opened. It can be observed that the interface shapes before overflow present some differences in each video but are overall pretty similar. However, strong variations are obtained after the overflow resulting in a selection of a very different volume in each experiment.

This being said, this master thesis will focus on the study of the volume before the overflow. This volume is key for two main reasons:

1. The experimenters do not want this volume to be sensitive to uncontrolled parameters.

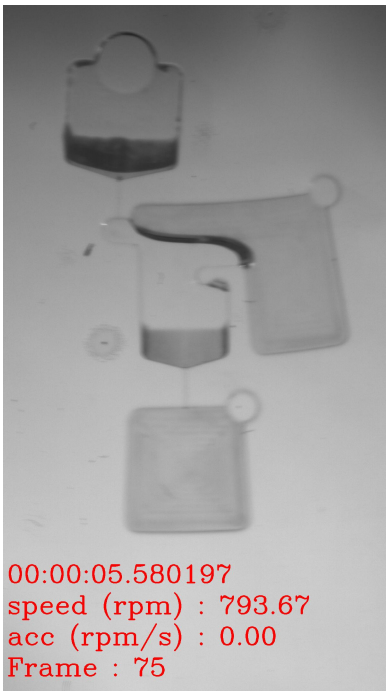

(a) One frame before the liquid flows in the waste chamber.

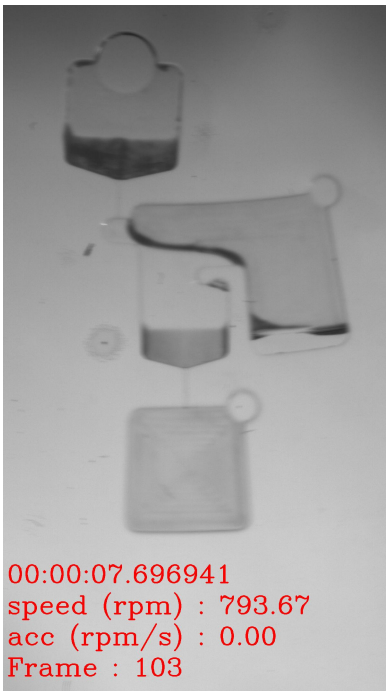

(b) One frame just before the valve under the right chamber opens.

Figure 2: Front view of the system and the liquid in one of the experiments made by the Microfluidic lab.

(a) One frame before the liquid flows in the waste chamber.

(b) One frame right before the valve the right chamber opens.

Figure 3: Front view of the system and the liquid in one of the experiment made by the Microfluidic lab. The experiment is different from the one presented in Fig. 2 but was carried out in exactly the same conditions.

2. The study of this volume is the necessary first step to predict interface shapes after the overflow.

This problem leads to a need to study the sensitivity of the volume in the metering chamber with respect to geometric and physical parameters that have to be chosen carefully. However, the design of this kind of LoD is extremely complicated and has a high cost of production [1]. It is why industries cannot afford big experimental procedures before getting the final product. Moreover, such shapes cannot be anticipated analytically, that is why one should look for a numerical prediction.

The problem will be modelled in two ways: by solving analytical equations describing the shape of the interface and by using the Surface Evolver (SE) program. This is a software tool used for simulating and analysing the behaviour of liquid and solid surfaces in three-dimensional space. This program has several main advantages. Surface Evolver's advantages include its versatility in handling a wide range of complex surface and interface problems, making it suitable for physics, materials science, and engineering applications. It excels in optimisation, efficiently determining equilibrium configurations using energy minimisation principles. The software automatically handles the meshing of the different surfaces of interest. It is open-source so the software is completely free. Finally, Surface Evolver offers high numerical efficiency in simulating systems with accuracy, making it a preferred choice to simulate the shape of the interface.

Furthermore, the numerical models developed in the scope of this master thesis should be a starting point to study the shape of the interface after the overflow.

However, the number of simulations needed to study the sensitivity of the volume with respect to several parameters is huge. The Surface Evolver model is not able to perform a lot of simulations for different sets of parameters in a reasonable amount of time so a reduced analytical model based on the equations describing the shape of the interface must be developed.

Moreover, the problem will be considered quasi-steady and the evolution of the fluid will be simulated by iteratively increasing the volume of liquid in the chambers until it flows into the waste chamber. Also, the entire process is done at a constant rotational speed. Therefore, only the centrifugal force, acting as an artificial gravity, is involved in the process.

The objectives of this master thesis are then multiple:

1. Develop an analytical model able to predict correctly the shape of the interface before the overflow.
2. Getting to grips with the Surface Evolver programme and use it to model the evolution of the fluid in the operation unit until it flows into the waste chamber. This model should also be a starting point to model the shape of the interface just before the valve opens.
3. On the basis of the models, study the sensitivity of the volume before the overflow with respect to well-chosen geometrical and physical parameters.

Methodology and Overview

Chapter 1 starts with a short theoretical background on microfluidic and numerical optimisation methods used in the scope of the different models. After that, Chapter 2 defines the specific geometry of the problem, introduces the different parameters of interest and presents the different assumptions that have to be made in order to model the problem numerically. On this basis, Chapter 3 defines the analytical problem and its numerical resolution. Results obtain with this model are presented and compared with the results of the experiments made by the Microfluidic lab. Then, Chapter 4 introduces the functioning of the Surface Evolver program and the modelling of the chamber's geometry and liquid. Shapes of interface obtained through the program are then represented and compared with the experiments and the result obtained through the analytical model. Using the models developed in Chapter 3 and 4, the sensitivity study is performed in Chapter 5. This chapter introduces the method used to determine the sensitivity of the volume in the metering chamber with respect to different variations of geometrical and physical parameters. Results are then presented and discussed. Finally, the effect of a specific parameter, the height of the top wall of the metering operation unit, is studied in Chapter 6.

CHAPTER 1

THEORETICAL BACKGROUND

This chapter focuses on establishing the theoretical background required for modelling the microfluidic metering chamber. First, the fundamentals of capillarity are discussed, introducing the notion of interface, contact angle, capillary length, surface free energy and its minimisation. This is followed by a description of the forces acting on a liquid in a Lab-on-Disk and the notion of equivalent centrifugal pressure. Then, this chapter also briefly presents the Surface Evolver program as well as the different numerical methods employed by the program, like the gradient descent, the conjugate gradient descent as well as the Newton-Raphson method.

1.1 Fundamentals of Capillarity

In general terms, capillarity is the phenomenon of interaction that occurs at the interfaces between two immiscible liquids, between a liquid and air or between a liquid and a surface. To understand where it comes from, the notion of interface and surface tension is introduced. Then, their implication on the behaviour of fluids at the microscale will be presented.

1.1.1 Interface

Schematically, an interface defines the boundary between two entities, in the present report, the boundary between two fluid domains. In practice, the interaction between the molecules of each fluid and Brownian diffusion, which represents thermal agitation, determine the border between the two immiscible fluids. [6]. When a liquid is in contact with a solid, a contact angle θ can be defined as the angle at which a liquid-vapour interface contacts a solid surface [7], as shown in Fig. 1.1.

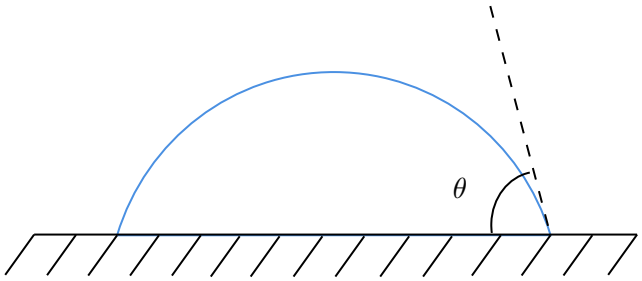

Figure 1.1: 2D view of the interface of a drop and contact angle θ. The drop is depicted in blue. Figure adapted from [7].

1.1.2 Surface tension

In a condensed state, molecules within a liquid exhibit cohesive forces, resulting in mutual attraction. Those situated in the bulk of the liquid experience interactions with neighbouring molecules on all sides, typically involving Van der Waals forces for liquids and hydrogen bonding for polar liquids like water. Conversely, molecules residing at an interface experience interactions within a half-space, interacting with molecules of the same liquid, while simultaneously interacting with molecules of another liquid or gas in the other space. As a consequence of these interactions, molecules away from the surface are equally pulled in all directions, nullifying the net force, as shown Fig. 1.2. However, surface molecules lack bonds on one side, so the surface tension is the energy cost (per unit area) for molecules to be at the interface.

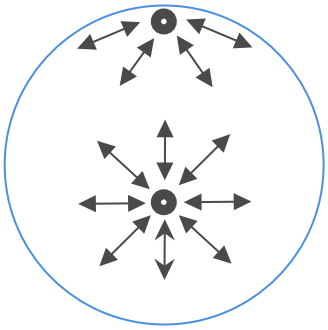

Figure 1.2: View of the cohesive forces on molecules (in gray) at the interface or in the drop (in blue).

The surface tension can also be interpreted as a force per unit length, which is always tangent to the liquid interface. The force applied on the solid is then:

$$\mathbf{F} = \sigma \oint_C \mathbf{n}\, \mathrm{d}l\,,$$

where C and $\mathrm{d}l$ indicates the the triple line, i.e the line where gas/liquid/solid phase are in contact, and $\mathbf{n}$ the normal to the triple line in the plane tangent to the liquid/gas interface. The force applied on a gas/liquid/solid interface can be visualised in Fig. 1.3.

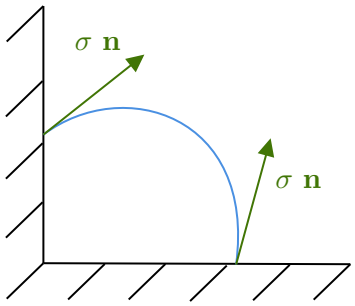

Figure 1.3: View of the forces (in green) on the triple line, induced by surface tension.

1.1.3 Capillary length

Now that the concept of surface tension has been established, it is interesting to introduce a number defining the shape of the interface at the microscale.

Surface tension and body forces both influence a fluid system, there is a characteristic length scale, named capillary length λ_c [m], at which these forces are matched:

$$\lambda_c = \sqrt{\frac{\sigma}{\Delta\rho g}}, \tag{1.1}$$

where $\Delta\rho$ [kg/m^3] is the density difference between the two fluids and g [m/s^2] the body forces. This number summarises the balance between capillary and body forces. In fact, surface tension dominates length scale smaller that λ_c and body forces larger scales. For example, a puddle smaller than λ_c will take the shape of a spherical cap, but if it is larger than the capillary length it will form a horizontal flattened interface.

1.1.4 Surface free energy

Another essential concept in interfacial phenomena is Surface Free Energy (SFE) [J/m^2]. It represents the work that would be necessary to increase the surface area of a solid phase. It is physically equivalent to surface tension but SFE is usually used for solid surfaces. This energy plays a central role in wettability, i.e. the ability of a liquid to maintain contact with a solid. In fact, every system aims at the lowest feasible free energy. Due to the surface tension, liquids take up the most minor surface area at a given volume and, in zero gravity, form spherical droplets. On the other hand, solids can create an interface with a liquid to lower free energy, i.e. they can be wetted, but they cannot reduce their surface via deformation.

1.1.5 Minimisation of the surface energy and minimal surfaces

When a system reaches equilibrium, it tends to minimise its total energy, including surface free energy. This principle underlies the formation of minimal surfaces, which are surfaces corresponding to the one of minimal energy. This minimisation is done under constraints imposed by external conditions, such as walls, fixed volume or fixed pressure.

The interface can then be calculated by minimising its surface energy. If a solid surface without any droplet is considered, the surface energy is [7]:

$$E_{\mathrm{SG},0} = \sigma_{\mathrm{SG}} S_{SG,0}$$

where $S_{\mathrm{SG},0}$ [m^2] is the solid surface in contact with the gas and $E_{\mathrm{SG},0}$ [$\mathrm{J/m}^2$] its energy. Then, a droplet is deposited on the solid and the total surface energy becomes a sum of surface energies:

$$E_\sigma = E_{\mathrm{LG}} + E_{\mathrm{SL}} + E_{\mathrm{SG},1}, \tag{1.2}$$

where E_{LG} is the surface energy of the liquid interface in contact with the gas, E_{SL} the surface energy of the liquid surface in contact with the solid and $E_{\mathrm{SG},1}$ the surface energy of the new solid surface in contact with the gas. Since $E_{\mathrm{SL}} = \sigma_{\mathrm{SL}} S_{\mathrm{SL}}$, $E_{\mathrm{SG},1} = \sigma_{\mathrm{SG}} S_{\mathrm{SG},1}$ and $S_{\mathrm{SG},1} = S_{\mathrm{SG},0} - S_{\mathrm{SL}}$, the equation 1.2 can be rewritten as

$$E_\sigma = E_{\mathrm{LG}} + S_{\mathrm{SL}}(\sigma_{\mathrm{SL}} - \sigma_{\mathrm{LG}}) + E_{\mathrm{SG},0}. \tag{1.3}$$

It must be noticed that, the term $E_{\mathrm{SG},0}$ does not depend on the drop shape so it does not come into play in the minimisation.

1.1.6 Contact angle - Young's Law

The different forces on the triple line between a liquid, a gas and a smooth surface can be sketched as in Fig. 1.4.

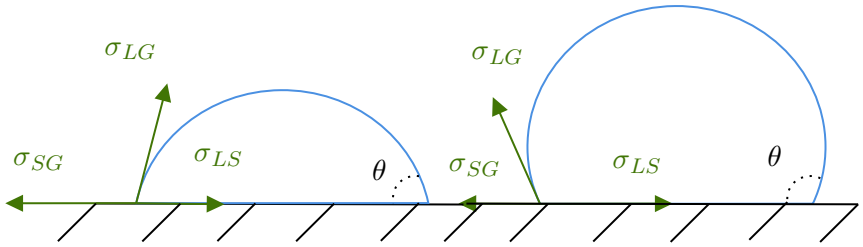

Figure 1.4: Schematic of the forces in equilibrium at the triple line. Hydrophilic case at left ($\theta < 90$), hydrophobic case at right ($\theta > 90$). σ_{SG} is the surface tension between the solid and the gas, σ_{LG} between the liquid and the gas and σ_{LS} between the liquid and the solid.

At equilibrium, the resultant of the force must be equal to zero. By projecting σ_{LG} on the horizontal axis, the following equation is obtained:

$$\begin{aligned} &\sigma_{SG} = \sigma_{SL} + \sigma_{LG}\cos\theta \\ \iff\ &\theta = \arccos\left(\frac{\sigma_{SG} - \sigma_{SL}}{\sigma_{LG}}\right). \end{aligned}$$

This equation is called Young's law [8] and θ is called the Young contact angle. It shows

that the contact angle θ is determined by the surface tensions between each constituent.

Moreover, this equation can be implemented into Eq. 1.3, so that

$$E_\sigma = \sigma_{\mathrm{LG}} S_{\mathrm{LG}} - \sigma_{\mathrm{LG}} S_{\mathrm{SL}} \cos\theta. \tag{1.4}$$

The surface tension of the solid is therefore not needed to minimise the surface free energy, the only parameters intervening in the equation are θ, the contact angle between the interface and the solid, and σ_{LG}, which can be measured quite easily.

1.1.7 Contact angle hysteresis and pinning

After the contact angle and Young's law have been introduced, it is interesting to look at contact angle hysteresis and pinning. Contact angle hysteresis refers to a phenomenon observed when a liquid droplet is in contact with a solid surface and the contact angle of the droplet changes as the droplet size increases or decreases or as the droplet moves on a surface. In simpler terms, it is the difference in the contact angle of a droplet as the contact line advances on a surface compared to when it recedes from the same surface. From this phenomena, two contact angles can be defined:

- **Advancing contact angle:** θ_{a}. The contact angle formed by the liquid and the solid when the contact line is advancing, illustrated in Fig.1.5a.
- **Receding contact angle:** θ_{a}. The contact angle formed by the liquid and the solid when the contact line is receding, illustrated in Fig.1.5b.

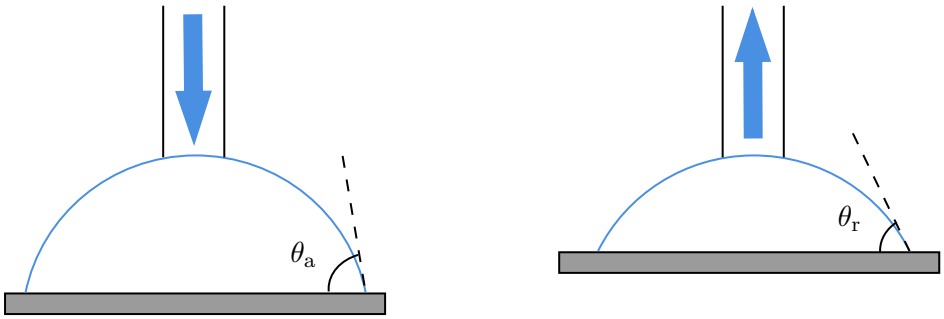

(a) The volume of the droplet is increased by a pipette, the contact line is advancing.

(b) The volume of the droplet is decreased by a pipette, the contact line is receding.

Figure 1.5: Representation of the advancing θ_{a} and reducing θ_{r} contact angle between a droplet whose contact line is advancing/receding on a flat surface.

This concept of hysteresis is due to local defects in the surface on which the liquid evolves [9]. Moreover, it can be said that

$$\theta_{\mathrm{a}} > \theta > \theta_{\mathrm{r}},$$

so that the advancing angle is larger than the contact angle given by Young's law, which can be intuitively explained by the fact that the liquid is slowed down by nano-inhomogeneities on

the surface. With the same idea, the receding contact angle is lower than θ since the liquid is pulled back by these inhomogeneities.

Pinning is when the liquid/gas interface is blocked in its motion because of a defect or discontinuity on the solid surface, it can therefore happen on an edge or due to finite contact angle hysteresis. In fact, the contact line does not move over the edge as long as the actual critical contact angle θ_2 is smaller than the limit $\alpha + \theta_1$, where α is the angle of the edge and θ_1 is the Young contact angle. The pinning condition can therefore be formulated as

$$\theta_1 < \alpha + \theta_2,$$

and is illustrated Fig.1.6

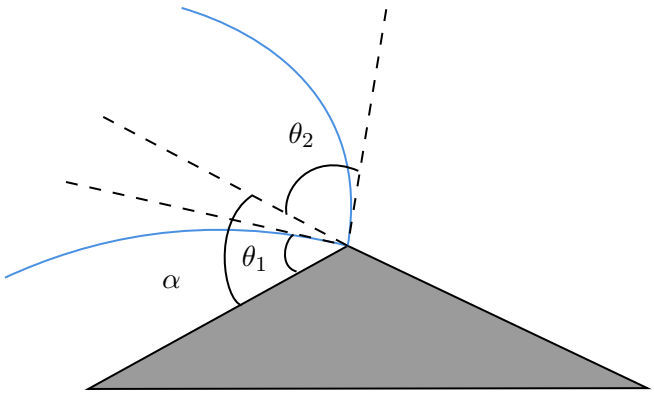

Figure 1.6: Droplet pinning on an edge. Figure adapted from [7].

1.1.8 Laplace pressure - Laplace law

Now that the phenomena happening at the triple line have been explained, it is interesting to look at the interface's curvature between the two fluids. To explain the curvature of the interface, two concepts must be introduced: Laplace pressure and Laplace law.

First, Laplace pressure is the difference in pressure between the sides of a curved interface separating two fluid media, called Δp [Pa]. It is shown in Fig. 1.7

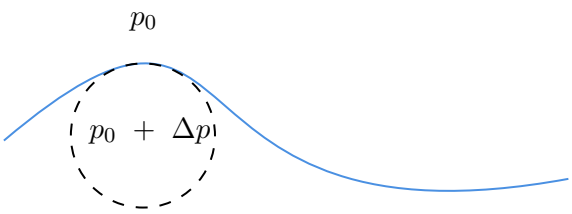

Figure 1.7: Schematic of the Laplace pressure. The blue curve represents a curved liquid interface, the liquid being below the curve. The dashed line represents the curvature of the interface. p_0 [Pa] is the pressure outside of the liquid and Δp is the Laplace pressure.

Secondly, the Laplace law is a fundamental principle in fluid mechanics that relates the Laplace pressure to the surface tension and curvature of the interface. This law is given by

$$\Delta p = \sigma \left(\frac{1}{R_1} + \frac{1}{R_2} \right) = \sigma \kappa, \tag{1.5}$$

where κ [m^{-1}] is the mean curvature and R_1 and R_2 [m] are the curvature radii. In simple terms, Laplace's law states that the pressure required to maintain a curved interface is proportional to the curvature.

1.2 Centrifugal Microfluidic

Now that the fundamental notions of microfluidic have been explained, it is interesting to look at the different body forces acting on a liquid in a Lab-on-Disk.

1.2.1 Body forces

The liquid is subject to inertial body forces that arise from the rotation of the disk. Since this rotation is controllable, the magnitude of these forces can therefore be tuned during an experiment. The three inertial body forces acting on a point-like body of mass m [kg] in a cylindrical system of coordinates are listed below:

1. **Centrifugal force $\mathbf{F_{Ce}}$:** The radial force induced by the rotation of the disk, given by:

   $$\mathbf{F}_{\mathrm{Ce}} = m\Omega^2 r \mathbf{e}_{\mathrm{r}},$$

   where $\Omega(t)$ [Hz] is the rotation speed, r [m] the distance between the centre of the disk and the centre of mass of the body. The rotation of the LoD induces a so-called artificial gravity g_{art} [m/s^2], which is given by

   $$\mathbf{g}_{\mathrm{art}} = \Omega^2 r \mathbf{e}_{\mathrm{r}}, \tag{1.6}$$

   so that the centrifugal force can be reduced to

   $$\mathbf{F}_{\mathrm{Ce}} = m\mathbf{g}_{\mathrm{art}}. \tag{1.7}$$

   It must be noted that the centrifugal force indeed depends on the radial position so that it can be considered to be similar to gravity only for a liquid staying approximately at a constant radial position, which will be the case of the interface studied in this thesis.

2. **Euler force $\mathbf{F_E}$:** As the whole experience takes place at constant rotational speed Ω, there is no Euler force acting on the liquid during the whole process.

3. **Coriolis force $\mathbf{F_{Co}}$:** Since the problem is treated as an evolution of the volume of the liquid without dynamic effect, the fluid has no relative velocity, which implies zero Coriolis force.

All these forces are represented Fig. 1.8.

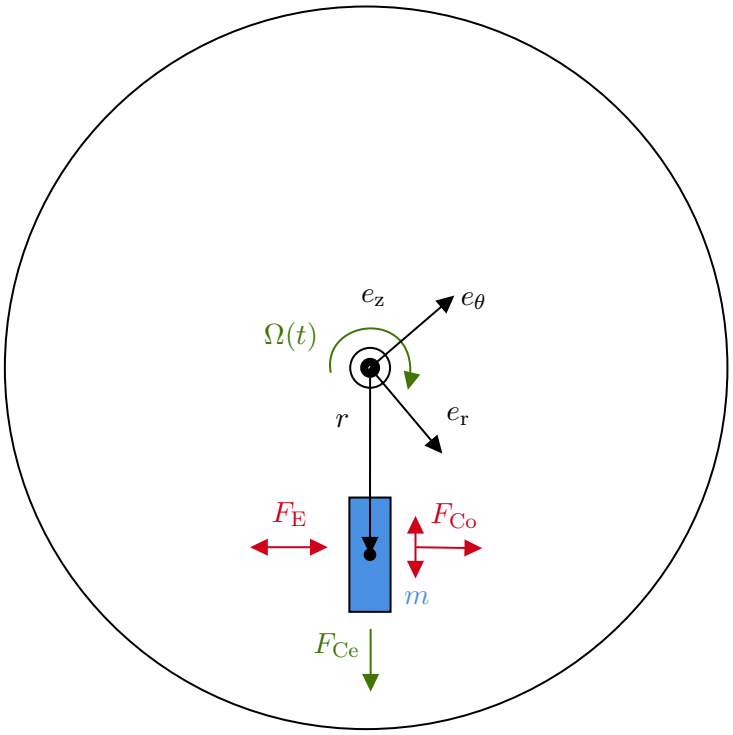

Figure 1.8: Schematic of the inertial body forces acting on a body of mass m. Only the green one has to be taken into account in the scope of this master thesis. Figure adapted from [5].

1.2.2 Centrifugal pressure.

From the rotation of the LoD at constant rotational speed Ω and quasi-static evolution of the fluid, a centrifugal pressure can be derived. Firstly, the Navier-Stokes equations in an inertial frame in the incompressible, constant rotational speed, quasi-static (no relative velocity $\mathbf{v}$ [m/s]) case can be written as

$$-\frac{1}{\rho}\boldsymbol{\nabla} p + \mathbf{g} - \boldsymbol{\Omega} \times (\boldsymbol{\Omega} \times \mathbf{x}) = 0,$$

where $\mathbf{x}$ [m] is the position and p [Pa] the pressure. In the Lab-on-Disk case, it can be said that

$$\begin{aligned} \boldsymbol{\Omega} &= \Omega \mathbf{e}_z, \\ \mathbf{x} &= x \mathbf{e}_r, \\ w &<< |\mathbf{u}|, \end{aligned}$$

the last equation comes from the fact that the disk is flat. The Navier-Stokes equation can therefore be adapted to

$$-\frac{1}{\rho}\boldsymbol{\nabla} p + \mathbf{g} + \Omega^2 r \mathbf{e}_r = 0.$$

From this equation, an equivalent centrifugal pressure can be derived as

$$-\frac{1}{\rho}\boldsymbol{\nabla} p + \Omega^2 r \mathbf{e}_\mathrm{r} = -\frac{1}{\rho}\boldsymbol{\nabla}\tilde{p} \iff \tilde{p} = p - \frac{\rho\Omega^2 r^2}{2} = \frac{\rho g_\mathrm{art} r}{2}.$$

This centrifugal pressure acts on the fluid inside the LoD so that this centrifugal contribution has to be taken into account in Laplace law stated in Eq. 1.5, resulting in a bending of the fluid in some subsystem of the chip.

Now that all the concepts needed to understand the physics of the studied system have been explained, it is interesting to look at the different numerical methods used to simulate the fluid's interface.

1.3 Numerical methods

This second part of the theoretical background deals with the numerical methods used by Surface Evolver in order to find the surface of minimal energy of an interface. Firstly, the program Surface Evolver is introduced. After that, the different numerical optimisation techniques used by the programme will be explained.

1.3.1 Surface Evolver

First of all, Surface Evolver [10] is a powerful software tool used for simulating and analysing the behaviour of liquid and solid surfaces in three-dimensional space. Created by Kenneth Brakke, it models and analyses the equilibrium configurations of interfaces by minimising the energy of a surface subject to constraints. The software computes the equilibrium shapes of surfaces, allowing for the simulation of, for example, droplets and their interface. The user can specify the initial geometry, boundary conditions and physical properties of the surfaces of interest in order to determine the shape of the liquid corresponding to the shape of minimal energy. The shape is meshed by SE, as shown in Fig. 1.9 and evolves toward its shape of minimal energy like in Fig. 1.10.

(a) Initial. (b) Meshed.

Figure 1.9: 3D surface automatically meshed by Surface Evolver.

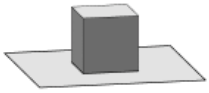

(a) Initial geometry.

(b) Shape of the droplet with no gravity.

(c) Shape of the droplet with $\theta = 135°$ and $g = 5$ in dimensionless unit.

Figure 1.10: Results obtained with Surface Evolver for a water droplet of volume $V = 1$, tension $\sigma = 1$ and density $\rho = 1$ in dimensionless unit.

1.3.2 Energy computation

Now that the general goal of Surface Evolver has been introduced, it is interesting to look at the mathematical equation minimised by the program in order to find the shape of minimal energy.

In fact, the total energy minimised by SE can be a sum of different energies [11]: gravitational, surface tension, squared mean curvature and user-defined surface integral. However, in this study only the surface energy and the gravitational energy have to be taken into account, so that the total energy to be minimised is the sum of these two energies. In Cartesian coordinate, the gravitational energy of a body B having a density ρ under an acceleration of gravity g is given by

$$E_{\mathrm{g}} = g\rho \iiint_B z \,\mathrm{d}V \,,$$

where $\mathrm{d}V$ [m^3] is the infinitesimal volume of the body B.

In practice, this energy is calculated using divergence theorem as

$$E_{\mathrm{g}} = g\rho \iint_{\partial B} \frac{z^2}{2} \vec{k} \cdot \mathrm{d}\vec{S} \,, \tag{1.8}$$

where ∂B is the boundary of the body B, $\mathrm{d}\vec{S}$ the infinitesimal surface of the boundary ∂B and $\vec{k}$ is the unit vector in the direction parallel and opposite to the body force.

Using Eq. 1.4 and Eq. 1.8, the total energy minimised by Surface Evolver is then:

$$E_{\text{tot}} = E_\sigma + E_{\text{g}} \tag{1.9}$$

$$= \sigma_{\text{LG}} \partial B_{\text{LG}} - \sigma_{\text{LG}} \iint_{\partial B_{\text{SL}}} \cos\theta \, \mathrm{d}S_{\text{SL}} + g\rho \iint_{\partial B} \frac{z^2}{2} \vec{k} \cdot \mathrm{d}\vec{S}\,, \tag{1.10}$$

where S_{LG} and S_{SL} from Eq. 1.4 has been renamed respectively to ∂B_{LG} and ∂B_{SL}.

Now that the equation to be minimised has been introduced, the minimisation can be done by evolving the surface down the energy gradient. In order to do that, several numerical optimisation scheme used by Surface Evolver will be presented.

1.3.3 Gradient descent

Finding a local minimum of a differentiable function can be done using the first-order iterative optimisation process known as gradient descent. It is the most simple numerical optimisation schemes used by SE.

This approach works by iteratively changing the input variables in the direction of the function's negative gradient. The algorithm starts with an initial guess for the input variables and computes the gradient. By moving in the opposite direction of this gradient, steps towards the minimum of the function are taken. This process continues until it converges, i.e. when the method reaches a point where the gradient is close to zero, indicating that we are close to the minimum of the function.

For example, considering a differentiable function $f(x)$, starting from an arbitrary point x_0, the iteration sequence is constructed as

$$x^{k+1} = x^k - \gamma d,$$

where x^{k+1} is the value of x at the previous iteration, x^k the computed value of x at the current iteration, $d = \boldsymbol{\nabla} f(x^k)$ the direction of the step, and $\gamma > 0$ is the length of the steps in this direction, called the learning rate. The learning rate can either be fixed or computed each iteration. The algorithm used to compute the learning rate is called a line-search algorithm.

Finally, the gradient descent method is illustrated Fig. 1.11.

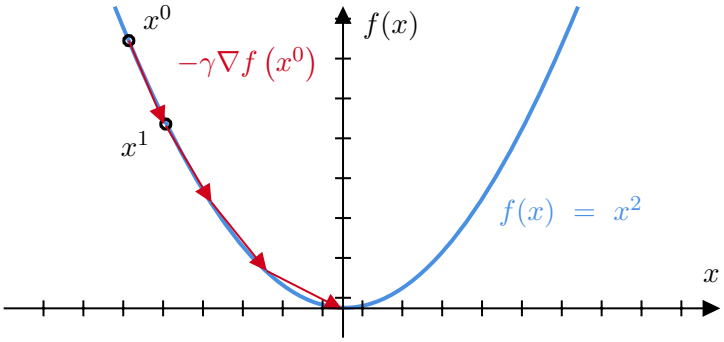

Figure 1.11: Illustration of the gradient descent algorithm on a function $f(x) = x^2$.

1.3.4 Newton-Raphson

The last numerical method presented is the Newton method, also called Newton-Raphson method. It is an iterative method used to find the zero of a function. This method can be illustrated by taking its most simple form which considers a differentiable single-variable function $f(x)$, where x is a real variable. By starting from an initial guess x_0, the algorithm evolves towards the root of the function by performing the following iteration scheme [12]:

$$x^{k+1} = x^k - \frac{f(x^k)}{f'(x^k)}.$$

This iteration scheme can be interpreted geometrically: the function $f(x)$ is replaced by its tangent at $(x^k, f(x^k))$ and the next iterate is defined by the interception of this tangent with the x-axis. It is illustrated Fig. 1.12.

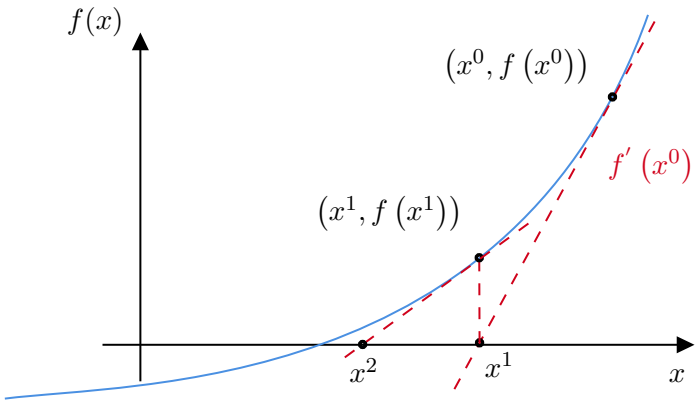

Figure 1.12: Illustration of the Newton-Raphson method on an arbitrary differentiable single-variable function $f(x)$. Figure adapted from [12].

The two methods presented there above will be used in the Surface Evolver program in order to minimise the total energy of the liquid and find the corresponding interface while respecting defined constrains.

CHAPTER 2

EXPERIMENTS AND PROBLEM DEFINITION

Now that the theory has been established, this chapter focuses on the problem that will be dealt with in this master thesis. Firstly, the principle of the experiments is recalled. Then, the exact problem of this thesis is defined. Furthermore, the chamber's geometry is parameterised and the different geometrical and physical parameters of interest are identified. Based on these parameters, dimensionless groups are formed. Finally, a simplification of the geometry is introduced and different assumptions required to model the problem are settled.

2.1 Experiments

Before any numerical model, several experiments have been performed in the context of the Medicare project. The tested metering operation unit works as the one described in the introduction. The liquid fills a metering chamber and then flows into a waste chamber. After that, the remaining liquid of the metering chamber is used to perform the desired analysis. The purpose of this operation unit is to always have the same amount of remaining liquid in the metering chamber so that the analysis is easily reproducible. A precise schematic of the unit operation used in the experience is presented Fig. 2.1.

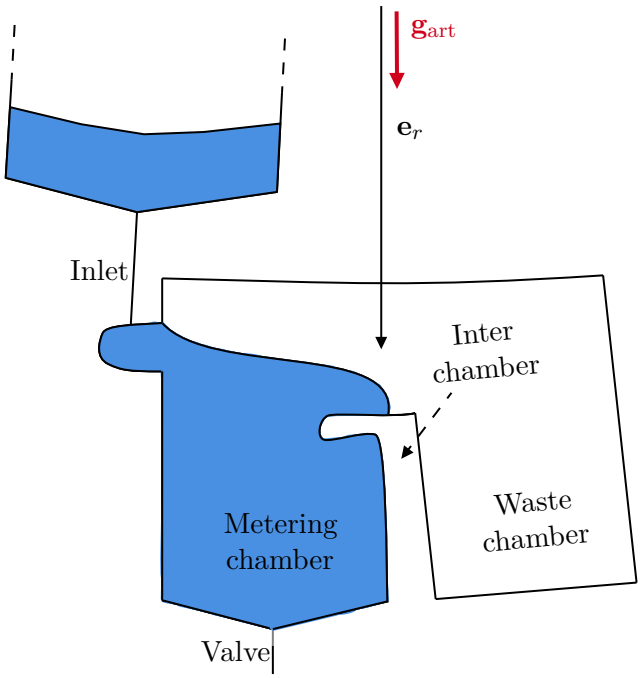

Figure 2.1: 2D representation of the metering operation unit used during the experiments performed in the context of the Medicare project. The liquid is depicted in blue. The operation unit is slightly curved so that the artificial gravity induced by the rotation of the disk acts perpendicularly to the liquid and the operation unit.

As mentioned in the introduction, these experiments highlighted that the shapes of the interface liquid air highly interfere with the metering process. However, the shape of the interface cannot be easily predictable analytically so a numerical study must be carried out.

2.2 Problem definition

As mentioned in the introduction, the experiments carried out by the Medicare team showed that the volume sensitivity was correlated to the shape of the interface. Like explained Sec. 1.1, the shape of the interface depends on the total energy of the liquid. The main goal of this thesis is then to study numerically the sensitivity of the total energy of the liquid, and so the sensitivity of the volume and shape of the interface, with respect to geometrical and physical parameters of the metering operation unit.

As stated Eq. 1.9, the total energy of the liquid results from the sum of the surface energy and the gravitational energy. The first one depends on the surface of contact between the liquid and the air but also on the liquid-solid surface of contact. Therefore, geometrical parameters that modify these two surfaces of contact must be studied. Also, this energy intrinsically depends on the surface tension of the liquid, as well as on the contact angle it makes with the solid, which are therefore two physical parameters to look at. Moreover, the gravitational energy is proportional to the artificial gravity induced by the rotation of the LoD, which can be tuned by the user. This is more a centrifugal energy than a gravitational one. Finally, since the mass

impacts the centrifugal energy, it makes sense to be careful with the geometrical parameter increasing the volume of liquid before it overflows in the waste chamber.

This leads to a precise definition of the geometrical and physical parameters that impact the total energy, and so the volume of the fluid, and that are involved in the metering operation unit.

2.3 Geometrical parameters

In order to define the different geometrical parameters of interest more easily, the geometry of the chamber will now be represented with rectilinear top and bottom faces. Also, the inlet channel will not be modelled and a high solid wall is assumed on the left side of the metering chamber.

The liquid filling the operation unit can be decomposed into two parts, which will be called body 1 and body 2:

1. **Body 1**: The part that has filled the whole metering chamber and whose volume will not evolve during the rest of the experiment, represented in dark-blue Fig. 2.2. This part has no more contact with air so it presents no interface to study.
2. **Body 2**: The part depicted in light-blue Fig. 2.2, whose volume still increases during the experiment until it has overflown in the waste chamber. It presents the interface liquid-air that must be studied so only the evolution of the volume of this body will be explored.

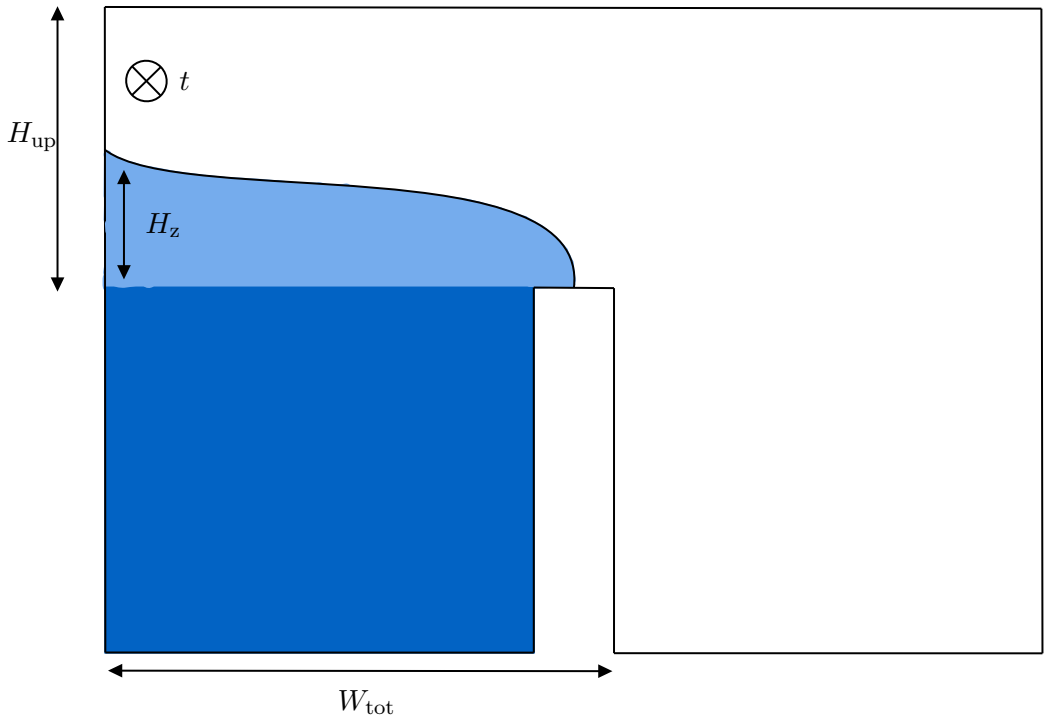

Figure 2.2: Metering operation unit used in Cartesian coordinate. The light-blue liquid is the liquid of interest since the volume of the blue liquid does not change once it has filled the metering chamber.

Once these two parts have been defined, geometrical parameters can be introduced as well as their impact on the interfaces, surface energy, and volume of body 2.

- W_{tot} [m]: It is the width between the left wall and the right corner of the inter-chamber. Increasing this parameter increases the volume of the liquid just before it has overflown, as well as the contact surface liquid-air and liquid-solid so that the total energy of the liquid given by Eq. 1.9 increases as well, which makes W_{tot} a parameter to be studied.
- H_{z} [m]: Height of the solid-liquid-gas contact line on the left plane with respect to the height of the liquid-liquid interface between body 1 and 2. This parameter can either be fixed or free to move. The first case corresponds to an evolution of the liquid volume with a pinned triple contact line on the left plane, as it can happen if an edge is placed at height H_{up} with respect to the inter-chamber. The other case corresponds to an evolution of the volume with a free triple line on the left plane, as if the left wall were smooth and without edges. This parameter directly influences the solid-liquid surface of contact, as well as the volume of the liquid when it has reached the left corner so that the impact of H_{z} must be studied.
- t [m]: Thickness of the operation unit. Again, it acts directly on the surface of contact between the liquid and the air and on the volume of the liquid when it has reached the left edge. Those two elements make t an additional geometrical parameter to study.
- H_{up} [m]: H_{up} is the difference of height between the inter-chamber and the upper border of the operation unit. This parameter is key: if it is too small, the liquid interface will connect to the top face rather than to the left face. If the fluid connects to the top wall the interface shape is totally different so this parameter has a different impact than the other on the evolution of the fluid. Therefore, a specific chapter will be dedicated to the influence of this parameter.

All these geometrical parameters are of the order of the millimetre so only volumes of the order of the millimetre cubed are used during the experiments.

2.4 Physical parameters

2.4.1 Artificial gravity

During the whole metering process, the rotational speed of the centrifugal LoD remains constant and is in first time set to 800 [RPM]. Moreover, the centre of the metering chamber is situated at a distance $R = 0.03$ m from the centre of the LoD. The distance between the centre of mass of the liquid filling the metering chamber and the centre of the LoD is considered to be equal to R. The artificial gravity induced by the rotation of the LoD along the radial axis can therefore be computed as Eq. 1.6:

$$g_{\text{art}} = \Omega^2 R = 210 \text{ m/s}^2,$$

where Ω [rad/s] is the rotational speed of the LoD. The rotational speed Ω and the distance between the centre of the operation unit and the centre of the LoD can both be easily modified. The artificial gravity is therefore a parameter that can be tuned by the experimenter and that will be studied.

Moreover, since the rotation of the LoD induces a high artificial gravity, the terrestrial gravity does not play a significant role in the evolution of the liquid inside the metering operation unit and will therefore be neglected in the rest of this master thesis.

2.4.2 Surface tension and contact angle

The ambient temperature during the whole experiment is 298 K. The fluid used to perform these experiments is water, whose density at 298 [K] is given by $\rho_{\mathrm{w}} = 997$ kg/m^3. The gas in the chambers is air, of negligible density. At this same temperature, the water surface tension is $\sigma_{\mathrm{w}} = 0.072$ N/m.

Moreover, the chambers are built with PMMA, which is a transparent thermoplastic. Thanks to the experiment made in [13], it is known that the contact angle θ_{PMMA} between PMMA and water lies in the range $[62 - 68][^\circ]$. However, the front wall of the operation unit is built with hydrophobic tape but for the sake of simplicity it will be regarded as PMMA in the models developed in this thesis.

As mentioned in section 1.1.3, the balance between gravitational force and surface tension can be summarised by the capillary length, which can be computed as

$$\lambda = \sqrt{\frac{\sigma_{\mathrm{w}}}{\rho_{\mathrm{w}} g_{\mathrm{art}}}} = 0.6 \text{ mm}.$$

This length is close to the different geometrical parameters of the operation unit, which are of the order of the millimetre. The capillary force plays therefore an important role in the shape of the meniscus. This is represented in Fig. 2.1 and this behaviour should be recovered in the numerical simulations. Since this balance highly influences the shape of the interface, the sensitivity of the volume with respect to the capillarity length will be studied.

2.5 Dimensionless groups

In order to carry out the study of the relative impact of the different physical and geometrical parameters on the sensitivity of volume just before the fluid flows into the waste chamber, dimensionless groups must be introduced. These parameters are defined on the basis of the parameters of interest identified, which have just been established. The key parameters of the problem are summarised below:

- θ [$-$]: The contact angle between the fluid and the walls of the operation unit.
- λ_{c} [L]: The capillary length, computed through Eq. 1.1, in which the artificial gravity g_{art} can vary.

- W_{tot} [L]: The total distance between the left wall and the right edge of the inter-chamber.
- H_{z} [L]: The height between the bottom of body 2 and its pinning on the left wall.
- t [L]: The deepness of the metering operation unit .

It leads to 5 parameters and 1 dimension ([L]) that have to be taken into consideration so that $5 - 1 = 4$ dimensionless parameters are needed. The 4 dimensionless parameters are then defined as

$$\begin{aligned}
\pi_1 &= \frac{H_{\text{z}}}{W_{\text{tot}}}, \\
\pi_2 &= \frac{\lambda_c}{W_{\text{tot}}}, \\
\pi_3 &= \theta, \\
\pi_4 &= \frac{t}{W_{\text{tot}}},
\end{aligned}$$

so the sensitivity of the critical volume will be studied with respect to these 4 parameters. Moreover, as explained in Sec.2.3, H_{up} has a specific impact on the evolution of the fluid inside the metering operation unit so it will be studied separately in Ch. 6.

2.6 Geometry and System of coordinate

The classic system of coordinates of a centrifugal LoD is a cylindrical system of coordinate, as depicted in Fig. 1.8. However, since the metering operation unit is far from the centre of the LoD, it can be described in a Cartesian system of coordinates, as shown in Fig. 2.3.

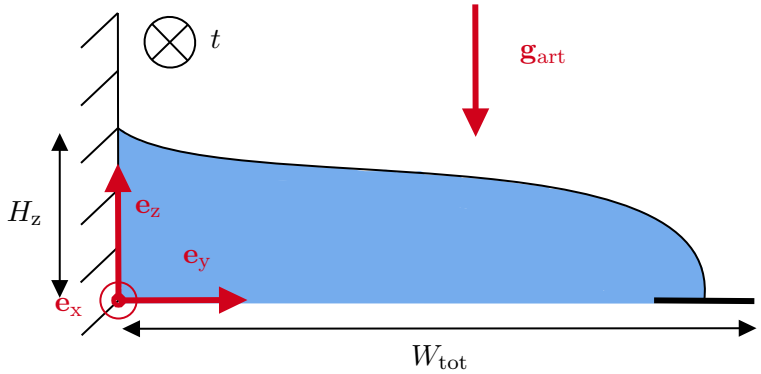

Figure 2.3: Representation of body 2 in Cartesian coordinate. The system of coordinates is centred on the bottom-left corner of the body, which does not move once the metering chamber has been filled. The black horizontal line represents the horizontal plane of the inter-chamber.

Moreover, as explained in Sec. 2.3, only the physics of body 2 is interesting, as it contains the water-air interface so only this part of the fluid will be taken into consideration.

As developed Sec 1.1, the only body force acting on the fluid is the centrifugal force, producing an artificial gravity $\mathbf{g}_{\text{art}}$. Thus, this is the only vector that depends on the coordinate system and whose expression must be adapted.

In cylindrical coordinates, the artificial gravity $\mathbf{g}_{\text{art}} = g_{\text{art}}\mathbf{e}_{\text{r}}$ is acting radially on the curved chamber, which means that it always acts perpendicularly to the fluid and to the curved top and bottom faces of the operation unit. It is therefore physically equivalent to represent the geometry of the chamber in Cartesian coordinates with rectilinear top and bottom faces and to rewrite $\mathbf{g}_{\text{art}}$ as $\mathbf{g}_{\text{art}} = -g_{\text{art}}\mathbf{e}_{\text{z}}$, so that the artificial gravity still acts perpendicularly to the fluid. and the metering operation unit.

2.7 Assumptions

Finally, in order to model the problem numerically, some assumptions have to be made.

2.7.1 Quasi-static problem

This assumption can be made because the speed of the displacement of the interface is very low during the filling of the operation unit. In fact, flow rates are of the order of the μL/s, and are regulated by the fluidic resistance of the channel upstream the metering chamber. Therefore, as the interface is of the order of the millimetre squared, its speed is less than a mm/s. Two dimensionless numbers defining the behaviour of the fluid can then be computed, the capillary and the Weber numbers.

Firstly, the capillary number Ca represents the balance between the viscous and capillary force and can be computed as

$$Ca = \frac{\mu V}{\sigma},$$

Where μ [Pa s] is the dynamic viscosity of the liquid, here water, and V [m/s] is the speed of the interface. Since the interface speed inside the operation unit is of the order of the millimetre per second, this number is several orders of magnitude below the unity. It can be concluded that viscous stresses have no impact on the shape of the interface. Secondly, the Weber number gives an indicator of how significant the fluid's inertia is in comparison to its surface tension and is defined as

$$We = \frac{2\rho L V^2}{\sigma},$$

where L is the characteristic length of the system, here of the order of the millimetre. Again, in the scope of the metering operation unit, the Weber number is several orders of magnitude below the unity, which indicates that the inertial effects are negligible.

Finally, the two remaining forces governing the interface shape are the body forces, here due to the centrifugal acceleration of the LoD, and surface tension.

2.7.2 Local pinning on edge

As the metering operation unit is three-dimensional, the liquid does not exactly pins over its entire triple line on the inlet corner of the chamber. However, in the scope of the models defined in this master thesis, this triple line will be considered straight along the entire depth of the operation unit.

CHAPTER 3

ANALYTICAL MODEL

In this chapter, the goal is to represent the shape of the interface water-air in the metering chamber by a set of equations that can be solved numerically. Once this system of equations has been established, the volume and total energy of the body 2 presented in Ch. 2 can be computed. From these equations and quantities, the shape of the interface water-air can be represented for different sets of parameters.

3.1 Analytical problem

Now that several assumptions have been made, the 2D curve representing the interface between water and air in the y-z plane can be mathematically described by a system of three Ordinary Differential Equations (ODEs). These equations define the evolution of the horizontal coordinate y [m], vertical coordinate z [m], angle φ [-] between the curve and the horizontal axis and local curvature κ [m^{-1}] in the plane $y-z$ with respect to a curvilinear parameter s [m]. The system is formulated as follows:

$$\begin{cases} \dfrac{\mathrm{d}y}{\mathrm{d}s} = \cos\varphi, & (3.1) \\ \dfrac{\mathrm{d}z}{\mathrm{d}s} = \sin\varphi, & (3.2) \\ \dfrac{\mathrm{d}\varphi}{\mathrm{d}s} = \kappa + \dfrac{2\cos\theta}{t}, & (3.3) \end{cases}$$

where θ is the contact angle between the liquid and the solid walls, κ [m^{-1}] is the curvature in the $y-z$ plane and the second term of the last equation is the curvature in the depth of the LoD. Then, an expression linking κ and the angle φ can be obtained by writing the equation of the pressure balance on the red contour depicted Fig. 3.1:

$$\sigma\kappa - \rho g \mathrm{d}z - \sigma(\kappa + \mathrm{d}\kappa) = 0 \iff \frac{\mathrm{d}\kappa}{\mathrm{d}s} = -\frac{\rho g_{\mathrm{art}}}{\sigma}\sin\varphi,$$

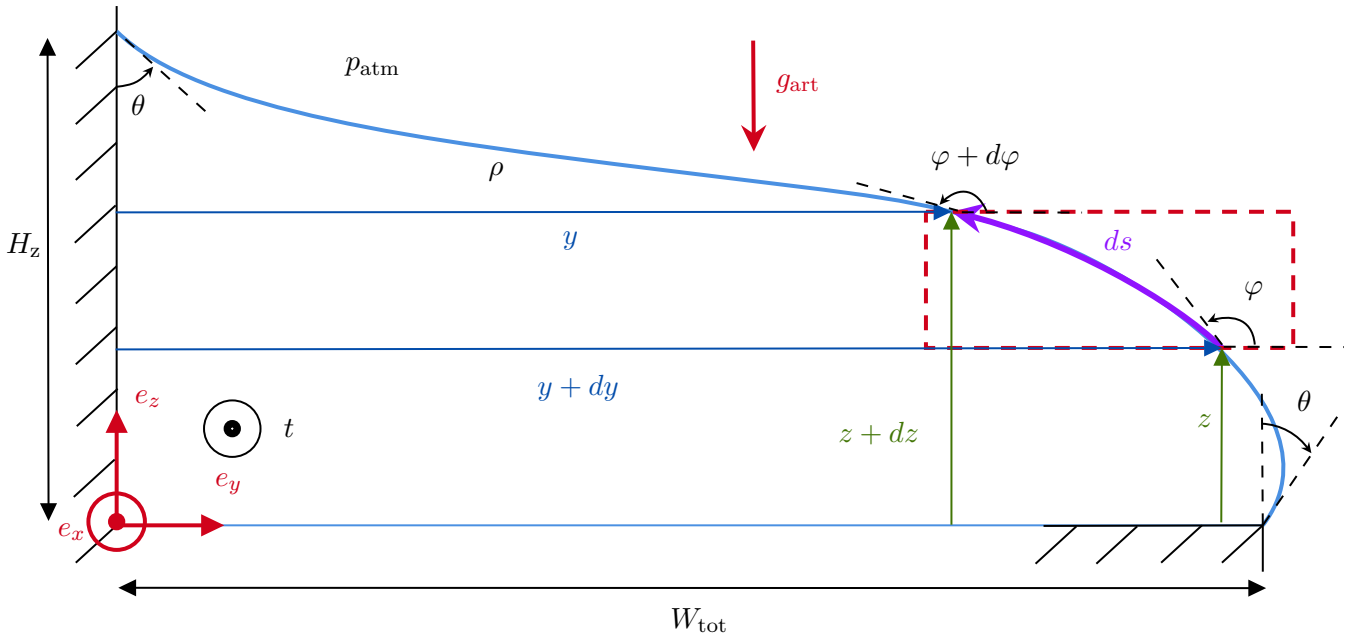

Figure 3.1: 2D View of the interface of the liquid in the first chamber. In blue, is the interface of the liquid. In red, is the contour of the pressure balance. ρ [kg/m^3] is the density of the liquid, p_{atm} [Pa] is the atmospheric pressure and $\theta°$ is the contact angle between the fluid and the solid. The left wall of the metering chamber is placed at $y = 0$ and the intersection between the water interface and the left wall at $z = H_z$. $y = W_{\text{tot}}$ corresponds to the left corner of the inter-chamber and its height is placed at $z = 0$. Finally, $x = 0$ and $x = t$ correspond respectively to the back and front plane of the LoD.

with σ the surface tension between both fluids, here the surface water-air tension. Using equation Eq. 3.2 the pressure balance can be rewritten as

$$\frac{\mathrm{d}\kappa}{\mathrm{d}s} = -\frac{\rho g_{\text{art}}}{\sigma}\frac{\mathrm{d}z}{\mathrm{d}s} \iff \kappa = \kappa_0 - \frac{\rho g_{\text{art}}}{\sigma} z. \tag{3.4}$$

By replacing Eq. 3.4 in Eq. 3.3, the system describing the water-air interface is then:

$$\begin{cases} \dfrac{\mathrm{d}y}{\mathrm{d}s} = \cos\varphi, & (3.5) \\ \dfrac{\mathrm{d}z}{\mathrm{d}s} = \sin\varphi, & (3.6) \\ \dfrac{\mathrm{d}\varphi}{\mathrm{d}s} = \kappa_0 - \dfrac{\rho g_{\text{art}}}{\sigma} z, & (3.7) \end{cases}$$

where the last equation depends on a constant term κ_0 [m^{-1}], in which the second term of the Eq. 3.3 has been incorporated. This last equation brings together the effects of external factors such as the artificial gravity g_{art}, liquid density ρ, and surface tension σ, which influence the shape and behaviour of the water-air interface.

The goal of this analytical approach is to solve this system of ODEs for various values of κ_0 and find all the values of κ_0 that describe an interface that respects certain boundary conditions.

Once all valid κ_0 has been found, the associated interface corresponding to the one of minimal total energy is searched. In fact, this interface corresponds to the one observed physically.

Unfortunately, the system of ordinary differential equations cannot be solved analytically due to its complex nature. It is mathematically difficult to extract explicit solutions to the system since it consists of three interrelated equations with intricate relationships and non-linearities. In order to solve the system, numerical approaches are therefore required.

3.2 Numerical resolution

3.2.1 Problem solved as an IVP

To solve this system numerically, the problem is first expressed as an Initial Value Problem (IVP). The values of y, z and φ at $s = 0$ are given by the user. Those values represent the right edge of the inter-chamber, where the interface is pinned. $y(s = 0)$ represents then the distance W_{tot} between the left wall of the operation unit and the right corner of the inter-chamber. $z(s = 0)$ represents the height of the inter-chamber but is set at 0 here. Finally, since φ corresponds to the angle between the curve and the horizontal plane, $90° - \varphi(s = 0)$ represents the contact angle θ between the water on the right corner of the inter-chamber and the vertical. In fact, it corresponds to the angle θ_2 presented in Sec. 1.1.7, i.e. the angle between the fluid and the corner just before the fluid begins to move beyond the corner. It also corresponds to the contact angle on the left wall between the solid and the fluid, as depicted in Fig. 3.1. Finally, the initial conditions are:

$$\begin{aligned} y(s = 0) &= W_{\text{tot}}, \\ z(s = 0) &= 0, \\ \varphi(s = 0) &= 90° - \theta. \end{aligned}$$

To solve this initial value problem, the `solveivp` Python function is used. It is a numerical integration tool provided by the `scipy.integrate` module. In practical terms, it uses the Runge-Kutta method to approximate the values of the dependent variables at discrete position points.

The idea is then to define desired boundary conditions and solve this initial value problem on a range of s bigger than necessary for each κ_0 in a defined range. Then, check if the solution verifies the boundary conditions that will be presented at the next section at a certain s. If it does, the κ_0 corresponding to the solution is stored and κ_0 is incremented so that the next iteration begins. If it does not, κ_0 is directly incremented and the next iteration begins. This process is repeated on a whole range of tested κ_0.

3.2.2 Boundary conditions

Based on this method, it is interesting to look at 2 different sets of Boundary Conditions (BC). For both sets, y will be bounded to $y(s_{\max}) = 0$ m. $s_{\max}$ is the value of s where the boundary conditions are verified, which therefore will always correspond to the value of s on the left wall of the metering chamber, situated at $y = 0$.

The first set of BC adds a boundary condition on z so that $z(s_{\max}) = H_z$ corresponds to a static pinning on the left wall of the operation unit.

The second set of BC defines a condition on φ instead of z, so that $\varphi(s_{\max}) = \theta$. All those sets of boundary conditions are summarised Tab. 3.1.

	$y(s_{\max})$	$z(s_{\max})$	$\varphi(s_{\max})$
	m	m	–
Boundary conditions 1	0	H_z	Free
Boundary conditions 2	0	Free	θ

Table 3.1: Sets of boundary conditions

Moreover, a constraint on the volume can be associated with the simple condition $y(s_{\max}) = 0$. The shape of the interface and the corresponding k_0, as well as $z(s_{\max})$ and $\varphi(s_{\max})$ will therefore take values that give the required liquid volume.

If several κ_0 respect the boundary conditions or volume constraint, the total energy of the liquid must be computed and the curve corresponding to the one of minimal energy must be found.

Moreover, those boundary conditions cannot be achieved with a precision of 100% as it depends on the precision of the numerical scheme. The results are then obtained with an error of maximum 1% on the fixed boundary conditions.

3.3 Volume and Energy computation

Knowing that the area A under the curve $z(y)$ is given by

$$\mathrm{d}A = z\,\mathrm{d}y$$

the volume of the body 2 is then

$$V = At.$$

It must be notated that the transversal curvature $2\cos\theta/t$ has not been taken into account in the computation of the volume. In fact, the influence of the curvature along the depth of the metering operation unit will be studied thanks to the 3D Surface Evolver model. The contact angles between the front and back walls of the LoD and the liquid will therefore be considered equal to 90° in the analytical model, resulting in a zero-curvature along x.

Also, the total energy of the liquid is given by Eq. 1.9, i.e. it is equal to the sum of the gravitational and the surface energy of the liquid. Firstly, the gravitational energy can be computed as

$$E_{\mathrm{g}} = \rho g \int_0^{s_{\max}} z \,\mathrm{d}V = \rho g \int_0^{s_{\max}} z \,\mathrm{d}z \,\mathrm{d}x \,\mathrm{d}y \tag{3.8}$$

$$= \rho g t \int_0^{s_{\max}} \frac{z^2}{2} \,\mathrm{d}y \,. \tag{3.9}$$

Secondly, the surface energy must be computed. By adapting Eq 1.4 to the problem, the surface energy to minimise is given by:

$$E_\sigma = \sigma_w S_{\mathrm{LG}} - \sigma_w \cos\theta S_{\mathrm{SL}},$$

where θ is the contact angle of the interface PMMA-water, defined Sec. 2.4.2 and σ_{w} N/m the surface tension of water. Then the different contact surfaces must be defined with respect to the different geometrical parameters. The surface between the water and the air is equal to the length of the curve $s(y, z, \varphi, \kappa_0)$ corresponding to $s_{\max}$ multiplied by the depth t of the operation unit:

$$S_{\mathrm{LG}} = s_{\max} t.$$

Moreover, the surface of contact between the solid and the liquid can be decomposed into three parts. The first part corresponds to the surface of contact between the left wall and the liquid, equal to $H_{\mathrm{z}} t$. The second part is the contact surface between the liquid and the inter-chamber. Since it is considered that the liquid has already reached the right corner of the inter-chamber, it corresponds to $W_{\mathrm{ic}} t$, where W_{ic} [m] is the length between the left wall and the left corner of the inter-chamber. The third part is defined by the contact surfaces between the water and the back and front plane of the LoD, which are both given by A. Finally, the total surface energy can be written as

$$E_\sigma = \sigma_{\mathrm{w}} t s_{\max} - \sigma_{\mathrm{w}} \cos\theta (W_{\mathrm{ic}} t + H_{\mathrm{z}} t + 2A).$$

3.4 Results of the model

Now that the analytical problem, its numerical resolution, volume and energy have been established, the results of the model can be presented.

3.4.1 Boundary set 1 and comparison with experiments

A first result for the boundary condition 1 is presented in Fig. 3.2.

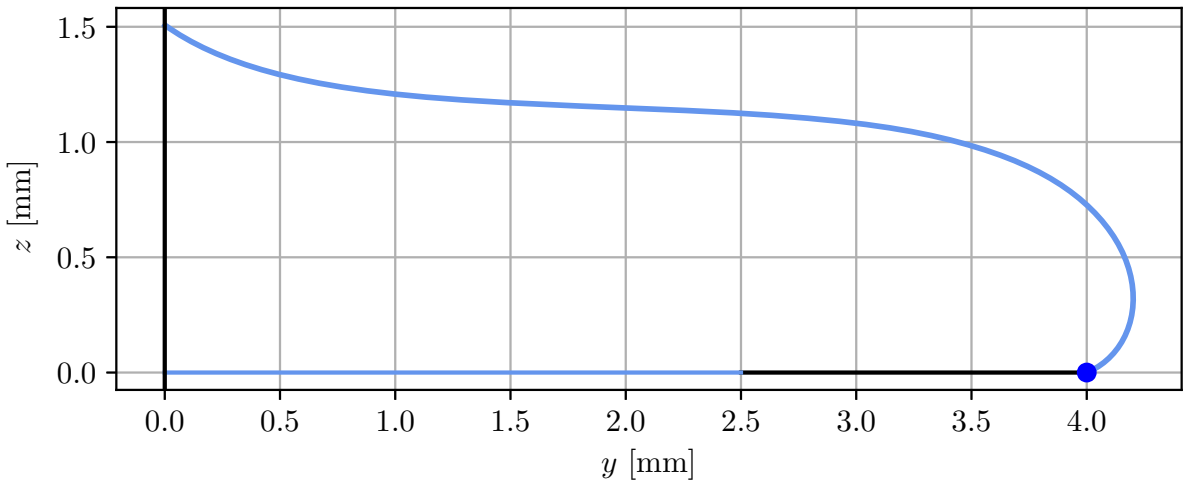

Figure 3.2: Shape of the interface water-air obtained from the numerical solution of the analytical problem constraint by the boundary set 1 and $H_z = 1.5$ mm. The interface is depicted by the blue curved line. The left wall of the metering operation unit is represented by the vertical black line on the left, the inter-chamber bottom face is represented by the horizontal black line and the contact surface between body 1 and body 2 is represented by the horizontal blue line.The different parameters are $W_{tot} = 4$ mm, $t = 1$ mm, $g_{art} = 210$ m/s^2 and $\theta = 68$ °.

It can be seen that the meniscus is vertically compressed while conserving a curved shape on the edge due to the capillary force. This is expected as an artificial gravity of $g_{art} = 210$ m/s^2 leads to a capillary length of $\lambda_c = 0.586$ mm so that an equilibrium between capillary and body forces must be found. This result can also be compared to the shape obtained through the experiments made by the Microfluidic lab, shown in Fig. 3.3.

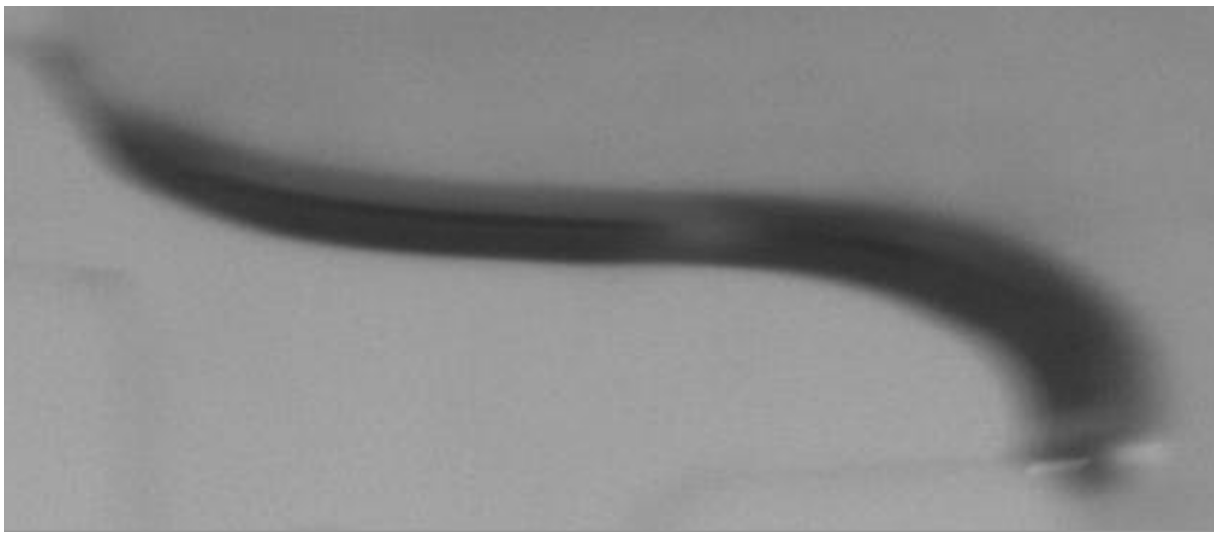

Figure 3.3: Front view of the interface just before the liquid begins to flow in the waste chamber, obtained through an experiment made by the Microfluidic lab with similar parameters as the one used in Fig. 3.2. The interface is depicted in black. The apparent width of the interface comes from its curvature in the depth of the operation unit, which has been neglected in the analytical model.

By comparing the two figures it can directly be seen that both shapes are very similar, confirming the ability of the numerical model to predict correctly the shape of the interface in the operation unit.

A result with a lower pinning on the left wall can also be obtained, as demonstrated Fig. 3.4.

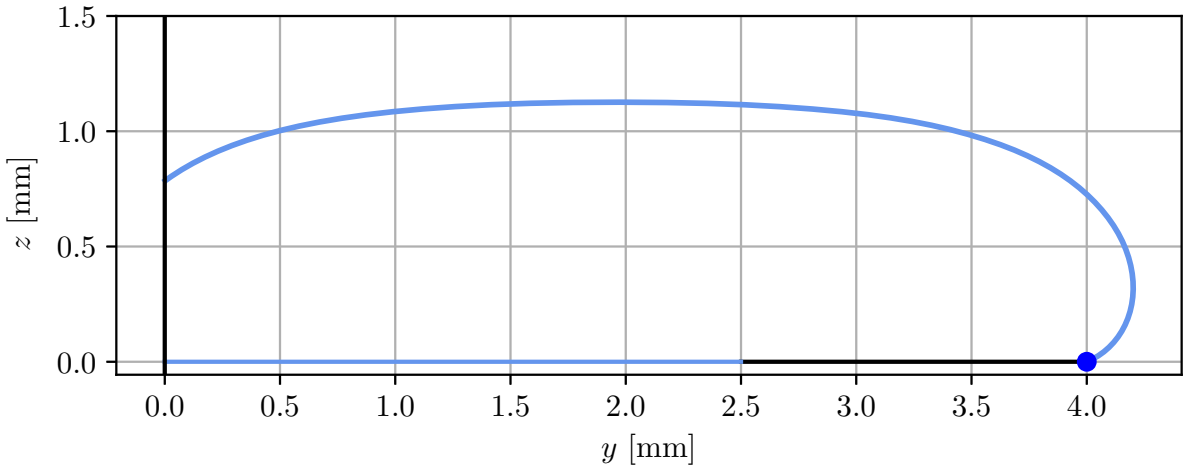

Figure 3.4: Shape of the interface water-air obtained from the numerical solution of the analytical problem constraint by the boundary set 1 and $H_z = 0.8$ mm. The different parameters are $W_{tot} = 4$ mm, $t = 1$ mm, $g_{art} = 210$ m/s^2 and $\theta = 68$ °.

It results in a more rounded shape since the pinning is lower on the left plane. This figure can be compared to another experiment carried out by the Microfluidic lab, where the interface is partially pinned on the lower edge of the inlet, shown in Fig.3.5. In fact, the interface is fully three-dimensional at this level, and considering 'point' pinning is a big approximation. But it is the only one that can be done simply in the analytical model. In subsequent iterations of the Microfluidic lab, the experimenters will extend the inlet of the metering chamber to force the pinning line to always be positioned at the same point, as it is considered in the numerical models presented here.

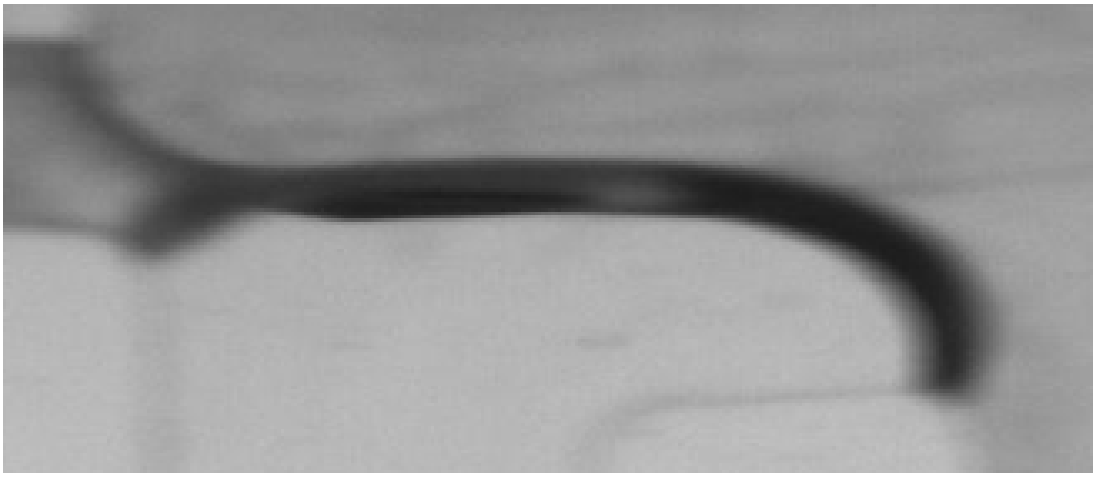

Figure 3.5: Front view of the interface just before the liquid begins to flow in the waste chamber, obtained through an experiment made by the Microfluidic lab with similar parameters as those used in Fig. 3.4..

3.4.2 Boundary set 2

Finally, shapes obtained with the boundary set 2, i.e. with a fixed contact angle on the left wall, are shown in Fig. 3.6.

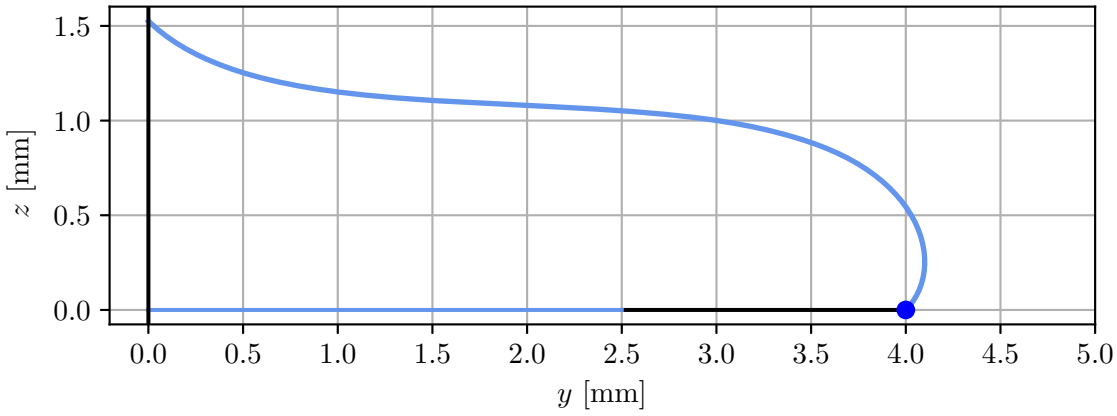

(a) $\theta = 45°$.

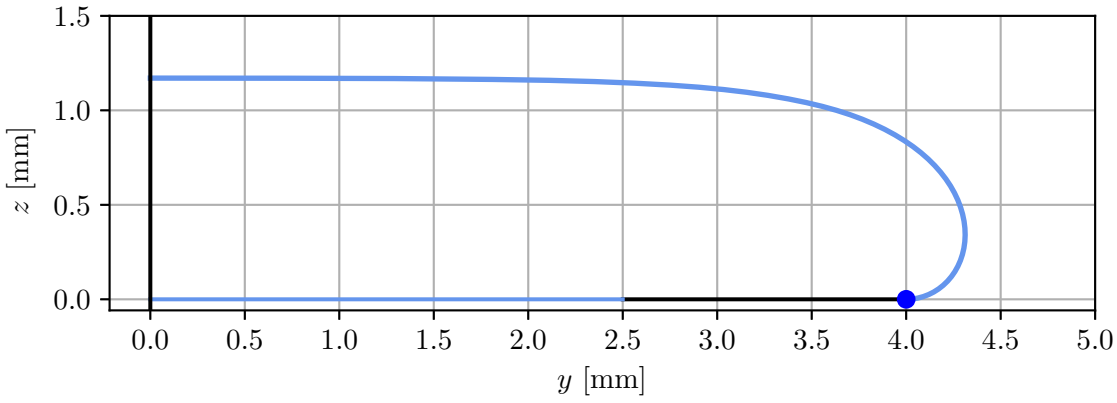

(b) $\theta = 90°$.

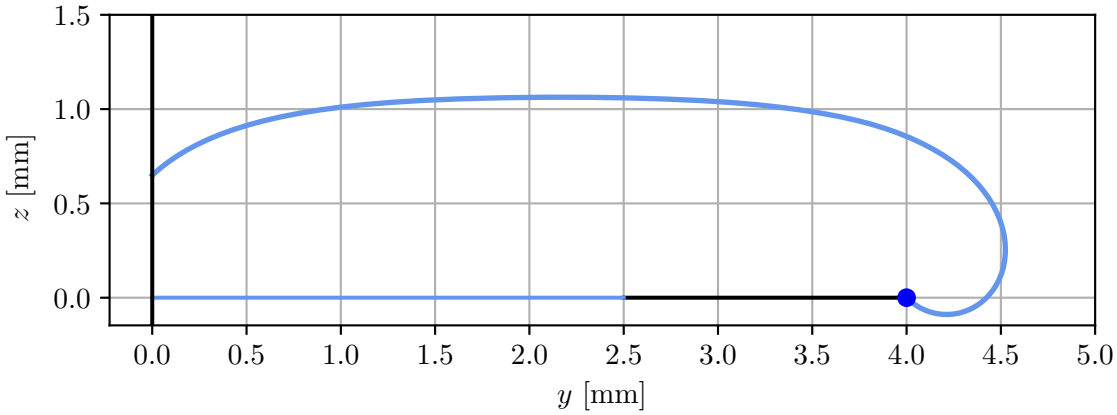

(c) $\theta = 135°$.

Figure 3.6: Shapes of the interface water-air obtained from the numerical solution of the analytical problem constraint by the boundary set 2. The different parameters are $W_{\text{tot}} = 4$ mm, $t = 1$ mm, $g_{\text{art}} = 210$ m/s^2.

CHAPTER 4

SURFACE EVOLVER MODEL

This chapter presents the Surface Evolver model used to study the shape of the interface taking into account the depth of the LoD . First, the geometry is modelled in the program. After that, the different constraints associated with the geometry as well as the way the energy is computed in SE is introduced. Then, the meshing and optimisation scheme are shortly described. Finally, the results obtained with the model are presented and compared with the results of the experiments as well as the with the analytical model results.

4.1 Surface Evolver utility

As explained in Sec. 1.3.1, Surface Evolver (SE) is a software tool used to simulate and analyse the behaviour of liquid and solid surfaces in a 3D space. The use of this program will help to analyse the impact of the curvature of the liquid due to the centrifugal pressure in the depth of the metering operation unit, which is not possible when using the analytical model.

4.2 Geometry

The metering operation unit as well as the liquid must be modelled in Surface Evolver. In order to do that the program allows to represent the various walls of the chambers as well as the initial configuration of the liquid by defining vertices, edges, faces and bodies in a Cartesian system of coordinates. Vertices are simply defined by a set of x, y and z coordinates. Edges are oriented segments defined by two vertices, their orientation is given by the order of definition of the two vertices. Thirdly, faces are made of a minimum of 3 edges and their normal depends on the orientation of the edges. If a face is composed of more than 3 edges, SE automatically meshes the face in order to represent it with triangles. Finally, bodies are composed of a set of faces connected by common edges. The body's faces have to be oriented so that all their normals are pointing inward or outward.

In the first instance, the liquid is defined by a body whose density corresponds to the one of the studied liquids, here water. This body is made of rectilinear faces and a desired volume

is specified. By running a convergence scheme, SE will mesh all the facets of the studied liquid. After that, in order to meet the force balance and reduce the free energy of the liquid-air-solid composite system, the triangles evolve and move to a different place in accordance with the geometrical constraints and the provided parameters, which can be contact angle, surface tension, density, volume of liquids, and gravitational field.

The modelled metering operation unit as well as the liquid filling the metering chamber can be visualised in Fig. 4.1.

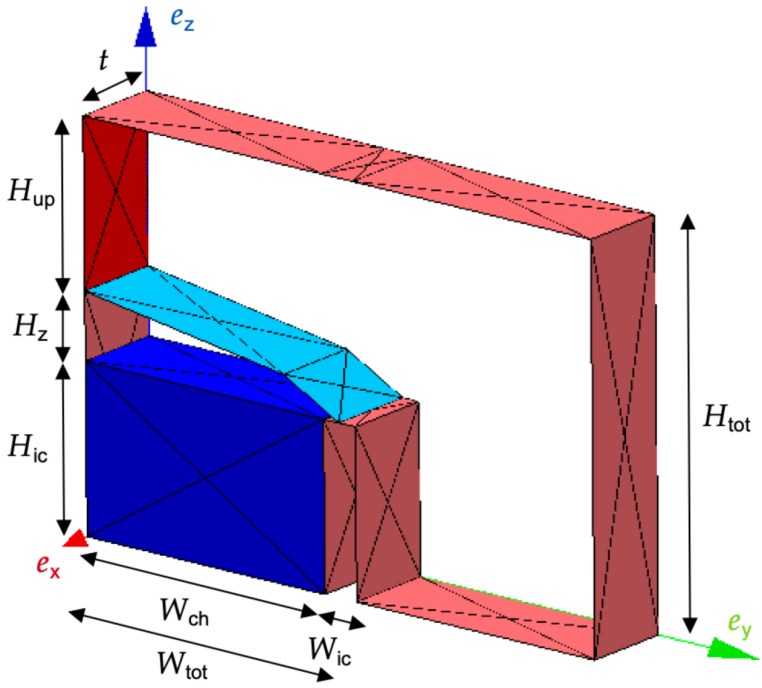

Figure 4.1: Metering operation unit modelled in Surface Evolver. The Cartesian system of coordinates is centred on the back left edge. H_{tot} [m] is the total height of the operation unit, H_{ic} [m] is the height of the inter-chamber and W_{ch} [m] is the width of the metering chamber. Those geometrical parameters are needed in order to define the constraints of the problem. The other geometrical parameters are the same as defined Sec. 2.3. Faces of Body 1 and 2 described in Sec. 2.3 are respectively depicted in dark-blue and light-blue. The different PMMA faces are represented in red. The front and back faces of the operation unit and body 2 are not represented visually but are only expressed through constraints, as will be explained in the next section. Also, the body 2 top face is divided into 2 sub-faces in order to facilitate convergence.

Initially, the most-right edge of body 2 is situated on the inter-chamber and not on its left corner as in Sec. 3. However, thanks to the capillary force simulated by Surface Evolver, this triple line will naturally move toward the inter-chamber right corner.

For the sake of simplicity and as it is not naturally displayed by Surface Evolver, the names e_{x}, e_{y} and e_{z} of the coordinate axis will not be indicated anymore. However, the red axe will always correspond to e_{x}, the green one to e_{y} and the blue to one e_{z}. Moreover, the different geometrical parameters will also not be displayed further in the report either, but when mentioned they will always refer to those presented in this section.

4.3 Constraints and energies

4.3.1 Constraints in SE

As mentioned in Sec. 1.3.1, Surface Evolver employs optimisation techniques to iteratively update the liquid surface shape, satisfying the geometrical constraints while minimising the total energy. Therefore, the liquid must be constrained in order to stay within the operation unit boundaries. In fact, the different faces in red in Fig. 4.1 are there for visualisation only, and the liquid stays in the chambers thanks to the constraints that simulates these different red planes. In the context of Surface Evolver, these constraints are specified using functions, allowing vertices to be constrained to the zero-level set of these functions [11]. One-sided constraints also exist, restricting a vertex to the region where the function has non-negative or non-positive values. Moreover, constraints can also be imposed on edges or facets, so that all vertices generated by subdividing them will inherit the same constraints.

When the vertex moves away from its constraints for any reason or if the vertex is not initialised on them, Newton's method, presented Sec. 1.3.4, is used to project the vertex on its associated constraints.

4.3.2 Energies in SE

As described Sec. 1.3.2, Surface Evolver total energy results from the sum of the gravitational energy and the surface tension energy, but the way these energies are declared in the program must be explained.

Surface energy

First of all, each facet can have a defined surface tension. Contact angles between liquid and walls can then be induced by facets that have different surface tension. However, this method is not the most efficient one and can slow down convergence, so other methods, called surface and edge integrals, must be introduced.

- **Surface integrals:** Facet's surface energy can be expressed as a vector field over the facet, which is computed as a surface integral. Gravitational energies of certain facets can also be defined as surface integral. In this case, facets are not represented visually and are not declared in the data file. In fact, their contribution to the optimisation problem is only defined by its geometrical constraint as well as its associated energy integrals along its edges.
- **Edge integrals:** As for the facets, the edge's energies can result from integrating a vector field as a line integral. This energy is associated with a constraint so that every edge resulting from the subdivision of the first one will inherit its line integral.

Gravitational energy

The gravitational energy computed by SE, expressed in Eq. 1.8, is taken over each bounding facet of a body. They are therefore surface integrand but handled internally by Surface Evolver.

However, they can be declared explicitly in edge or facet energy integrals, so that facets associated with this energy can be omitted.

Moreover, the volume content of omitted facet can be specified manually by giving the formula of the volume that should have been taken into account if the facet had not been omitted.

Now that constraints and associated energies in SE have been explained, those defining the operation unit and so the optimisation problem must be listed.

4.3.3 Constraints definition

As explained in the previous section, each constraint is defined by a function and an optional energy integrands and/or volume content. They can be listed as follows:

1. **Function:** $x = 0$. This constraint represents the back face of the LoD, situated at $x = 0$. An energy integrand must be associated with the edges to simulate the surface tension energy between the liquid and the PMMA wall. The edges of the back face of the liquid are represented in Fig. 4.2.

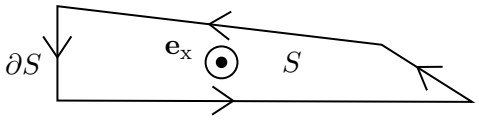

Figure 4.2: Oriented edges of the omitted back face of the liquid. Its normal points toward $\mathbf{e}_\mathrm{x}$. S denotes its surface and ∂S its boundary.

If the interface energy density between water and PMMA is expressed as $T = \sigma_w \cos\theta$, then the energy vector field $\mathbf{w}$ of this facet must be defined such that:

$$\iint_S T\mathbf{e}_\mathrm{x} \cdot \mathrm{d}\mathbf{S} = \int_{\partial S} \mathbf{w} \cdot \mathrm{d}\mathbf{l}\,.$$

By Green's Theorem, it is therefore needed that $\boldsymbol{\nabla} \times \mathbf{w} = T\mathbf{e}_\mathrm{x}$, so that the expression $\mathbf{w} = -T(z - H_\mathrm{ic})\mathbf{e}_\mathrm{y}$ is used in practice. In SE, each component of the vector field must be defined, so that the energy integrand associated with $x = 0$ is defined as

$$\begin{aligned}\mathbf{e_x} &: 0,\\ \mathbf{e_y} &: -T(z - H_\mathrm{ic}),\\ \mathbf{e_z} &: 0,\end{aligned}$$

where $-H_\mathrm{ic}$ comes from the fact that the lowest edge is at a height equal to $-H_\mathrm{ic}$ and this height is considered as the ground for this facet.

The same reasoning will be applied for the following constraints but will not be developed in detail.

2. Front vertical border of the LoD.
   Function: $x = t$
   Energy integrand:
   $$\mathbf{w} = T(z - H_{\text{ic}})\mathbf{e}_{\text{z}}$$

3. Maintain the left triple line on the inter chamber so that it does not go beyond.
   Function non-negative: $W_{\text{tot}} - y$, which is equivalent to $W_{\text{tot}} > y$.

4. Maintain the left triple line on the inter chamber so that it does not retract on body 1. For safety only as by capillarity the triple line should not retract.
   Function non-negative: $y - W_{\text{ch}}$.

5. Prevents the liquid from going beyond the upper border of the operation unit. For safety only as the liquid should flow in the waste chamber and not grow vertically as the volume increases.
   Function non-negative: $H_{\text{tot}} - z$.

6. Prevents the liquid upper faces from going beyond the back wall of the LoD.
   Function non-negative: x.

7. Prevents the liquid upper faces from going beyond the front wall of the LoD.
   Function non-negative: $t - x$.

8. Maintain the upper left edge of the liquid on the left wall of the operating unit.
   Function: $y = 0$
   Energy integrand:
   $$\mathbf{w} = -Tz\mathbf{e}_{\text{x}}$$

9. Bottom horizontal surface of body 2. Energy integrand also includes gravitational energy for the volume below the omitted contact facets.
   Function: $z = H_{\text{ic}}$
   Energy integrand:
   $$\mathbf{w} = \left(Ty + G_{\text{art}}\rho\frac{z^2}{2}y\right)\mathbf{e}_{\text{x}}$$
   Content: zy along the x axis.

10. For the triple line on right vertical facet. Used when the triple line has respected certain condition explained Sec .5.1.2.
    Function: $y = W_{\text{tot}}$
    Energy:
    $$\mathbf{w} = \left(T(H_{\text{ic}} - z) + Ty + G_{\text{art}}\rho\frac{H_{\text{ic}}^2}{2}y\right)\mathbf{e}_{\text{x}}$$
    Content: $H_{\text{ic}}y$ along the x axis

11. Maintain the triple line on the right vertical plane of the inter-chamber once it has passed its edge. It is used in order to do a smooth transfer of constraint when the triple line passes the left corner of the inter-chamber.
    Function: $y = W_{tot}$.

12. Prevent the liquid upper faces from going beyond the body 1 top face. For safety only.
    Function non-negative: $y - 0$.

13. Prevent the liquid left triple line from going upper the plane $z = H_{\text{ic}}$ once it has evolved beyon the right corner of the inter-chamber.
    Function non-negative: $H_{\text{ic}} - z$.

4.4 Meshing and Optimisation scheme

Now that the geometry and the constraints of the optimisation problem have been defined, the way the geometry is meshed must be presented.

Even if the triangulation is automatically handled by Surface Evolver, the refinement of the mesh can be controlled by the user. The mesh must be fine enough to allows the liquid to take smooth shapes. However, a mesh that is too fine can lead to bugs in SE, resulting in non-physical surfaces such as a surface that violates certain constraints.

Moreover, the user can define a script in order to perform grooming operations on the triangulated surface mesh. A script named `groom` has been written in order to refine edges longer than a given threshold, specified by the variable M_{l} [m]. One basic refinement operation corresponds to a division of the edge in two sub-edges and of the faces in four sub-faces. Simultaneously, the `groom` script deletes edges shorter than half M_{l} to simplify the mesh and reduce computational complexity. The smoothness of the interface will then be defined by variable the M_{l} that will be equal to 0.2 mm.

Furthermore, in order to achieve optimal edge positions resulting from triangulation, an optimisation scheme must be established. This process can be automated in Surface Evolver by employing the gradient descent algorithm that iteratively displaces the edges toward a position minimising the total energy of the system. While the gradient descent algorithm is internally implemented, the user retains control over the number of steps employed for the optimisation. Importantly, the user has the flexibility to perform gradient descent steps and mesh grooming in any order, allowing the construction of diverse convergence schemes. The evolution script to evolve the liquid from its initial configuration towards the desired volume is then the following:

1. The `groom` script is run 3 times in order to mesh the liquid's initial configuration.
2. 5 iterations of the gradient descent algorithm are run.
3. `groom` is run once.
4. Steps 2 and 3 are repeated 10 times.

5. The mesh is basically refined 1 time and M_l is divided by 2.

6. Steps 2 and 3 are repeated 10 times.

4.5 Results of the model

Now that the initial geometry, the different constraint as well as the optimisation scheme have been presented, it is time to show some results obtained with the Surface Evolver model.

4.5.1 Surface Evolver only

Firstly, it is interesting to look at the evolution between the initial geometry and a converged geometry, as shown in Fig. 4.3.

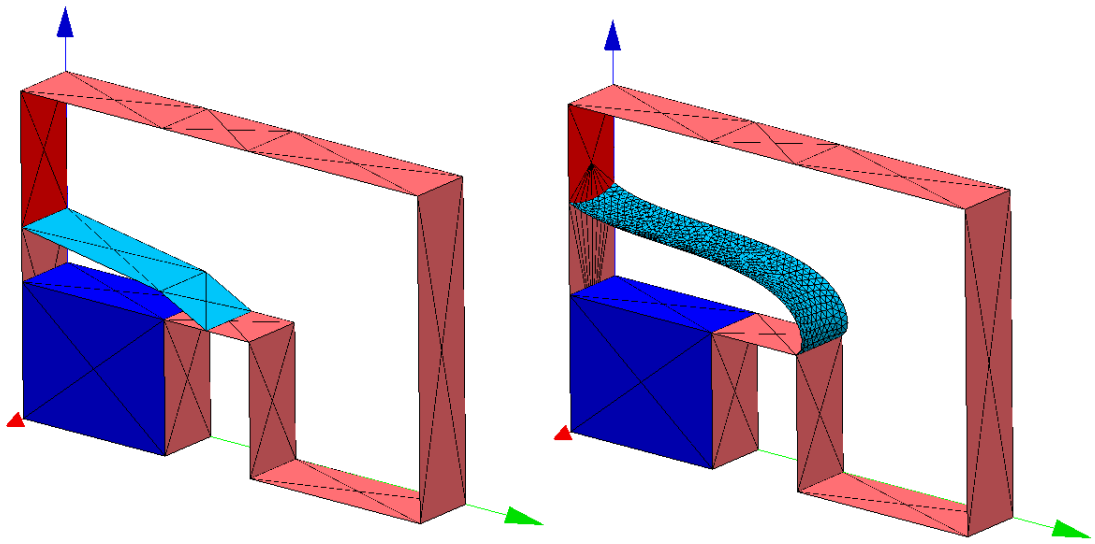

(a) Initial geometry $V = 2.56$ mm^3 (b) Final geometry, $V = 4$ mm^3

Figure 4.3: Initial and final geometry of body 2 in the SE model. $V_{\text{final}} = 4$ mm^3, H_z free, $W_{\text{tot}} = 4$ mm, $t = 1$ mm, $\theta = 68°$, $g_{\text{art}} = 210$ m/s^2.

It can be seen that due to capillary force, the triple line on the right has moved toward the right edge of the inter-chamber and the one on the left vertical wall has climbed. In fact, due to the contact angle hysteresis phenomena presented Sec.1.1.7, the contact angle between the liquid and the edge is increases when the liquid evolves on the edge before it flows into the waste chamber. Also, the interface has been meshed by SE and the different vertices have been moved in order to represent a volume of 4 mm^3 with an interface of minimal energy while respecting all the constraints imposed on the body. With the chosen parameters a capillary length of $\lambda_c = 0.586$ mm is obtained, so that the meniscus should be, and is, radially compressed while conserving a curved shape induced by Laplace pressure.

In this first results, the triple line situated initially at an height H_z on the left vertical wall was free to move vertically along the wall and ended after convergence at $H_z = 1.45$ mm. If this parameter is fixed at this value, the converged geometry shown in Fig. 4.4 is obtained.

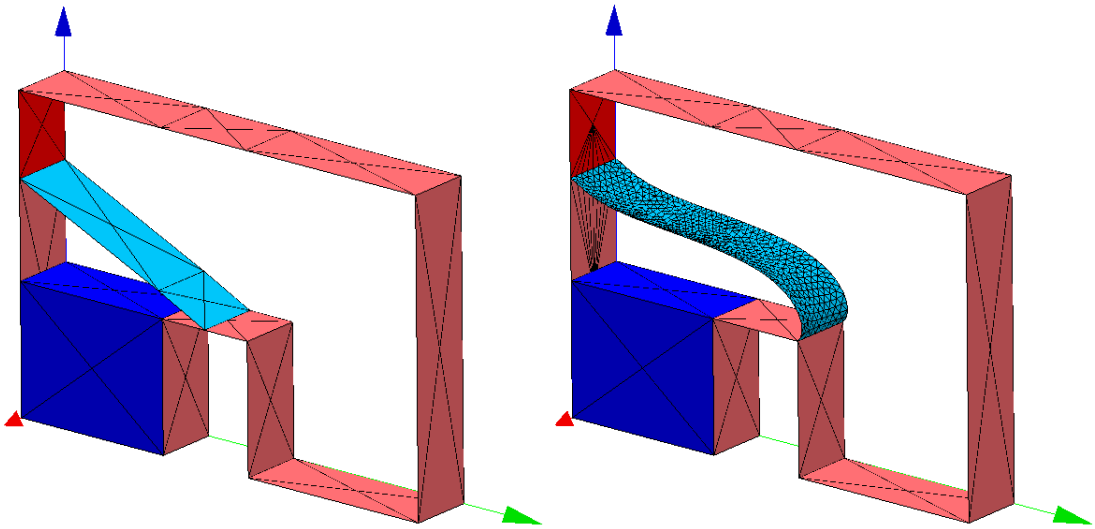

(a) Initial geometry, $V = 2.38$ mm^3. (b) Final geometry, $V = 4$ mm^3.

Figure 4.4: Initial and final geometry of body 2 in the SE model. $V_{\text{final}} = 4$ mm^3, $H_z = 1.45$ mm, $W_{\text{tot}} = 4$ mm, $t = 1$ mm, $\theta = 68°$, $g_{\text{art}} = 210$ m/s^2.

As expected, the result is very close to the one obtained when H_z was free to move. The only notable difference is that the left triple line does not present any curvature. This makes sense since this pinned triple line simulates a pinning on edge on the left part of the metering operation unit.

After that, it is interesting to look at the shape of the interface for different values of g_{art}, and so of λ_c. For example, if $g_{\text{art}} = 50$ m/s^2, which corresponds to a rotation of the disk of $N \approx 400$ RPM and $\lambda_c = 1.2$ mm, the shape in Fig. 4.5a is obtained. It can clearly be seen that the shape of the meniscus is much more curved than the previous shapes obtained with bigger g_{art}. Physically this result makes sense, in this case, $\lambda_c = 1.2 > 1$ mm so that surface tension dominates gravity and the shape of the meniscus is expected to be rounder.

Another example can be obtained with $g_{\text{art}} = 350$ m/s^2, which corresponds to a rotation of the disk of $N \approx 1030$ RPM and $\lambda_c = 0.45$ mm. In this case the shape depicted in Fig. 4.5 is obtained. This shape is much more flattened than the one with lower centrifugal gravity, translating the dominance of gravity on surface tension.

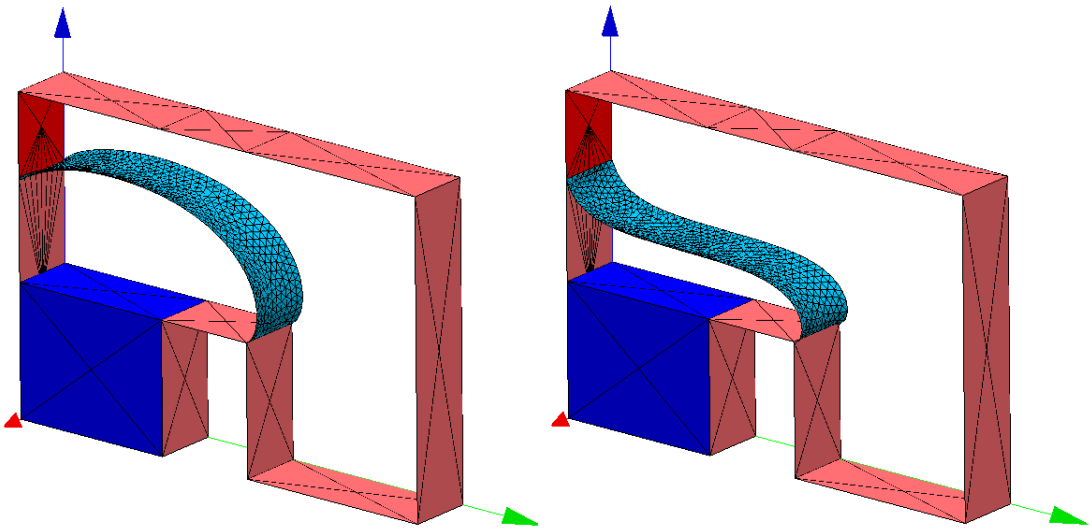

(a) $g_{\text{art}} = 50$ m/s^2. (b) $g_{\text{art}} = 350$ m/s^2.

Figure 4.5: Interface shape obtained with $g = 50_{\text{art}}$ m/s^2 and $g_{\text{art}} = 350$ m/s^2 just before the fluid begins to flow in the waste chamber. $H_z = 1.5$ mm, $W_{\text{tot}} = 4$ mm, $t = 1$ mm, $\theta = 68°$.

4.5.2 Comparison with the experiments

After that, it is interesting to look at the interface shape a few moments before the fluid begins to flow in the waste chamber, as shown in Fig. 4.6 and to compare the result obtained with the model to an experiment.

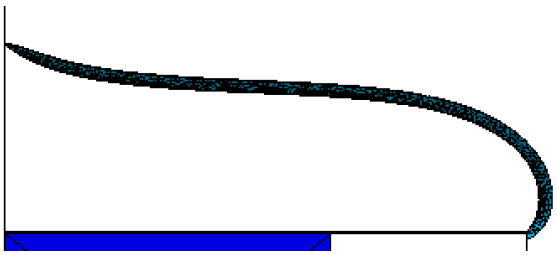

Figure 4.6: Front view of the interface shape obtained through Surface Evolver a few moments before it begins to flow into the waste chamber. The parameters are $H_z = 1.45$ mm, $W_{\text{tot}} = 4$ mm, $t = 1$ mm, $\theta = 68°$, $g_{\text{art}} = 210$ m/s^2.

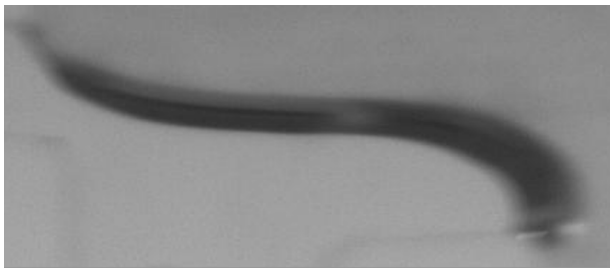

Figure 4.7: Front view of the interface just before the liquid begins to flow in the waste chamber, obtained through an experiment made by the Microfluidic lab with similar parameters as the one used in Fig. 4.6.

By comparing this figure to the one presented in Fig. 4.7, that shows the interface obtained

through an experiment carried out with similar parameters, it is obvious that both shapes are very similar, confirming the ability of the SE model to correctly predict the shape of the interface, and so the associated volume. Again, the apparent width of the interface observed in Fig. 1.10c and Fig. 4.5b comes from the bending of the meniscus in the e_x plane, induced by the equivalent centrifugal pressure introduced in Sec. 1.2.1.

4.5.3 Comparison with the analytical model

The shapes of the interface obtained with the analytical model and the Surface Evolver model can be compared. Fig. 4.8 shows the shape of the interface obtained by both models with the same parameters. It can easily be seen that both interfaces present very similar forms. Since both shapes have been obtained by using two very different approaches it confirms the accuracy of the models to predict the shape of the interface liquid-air in the operation unit.

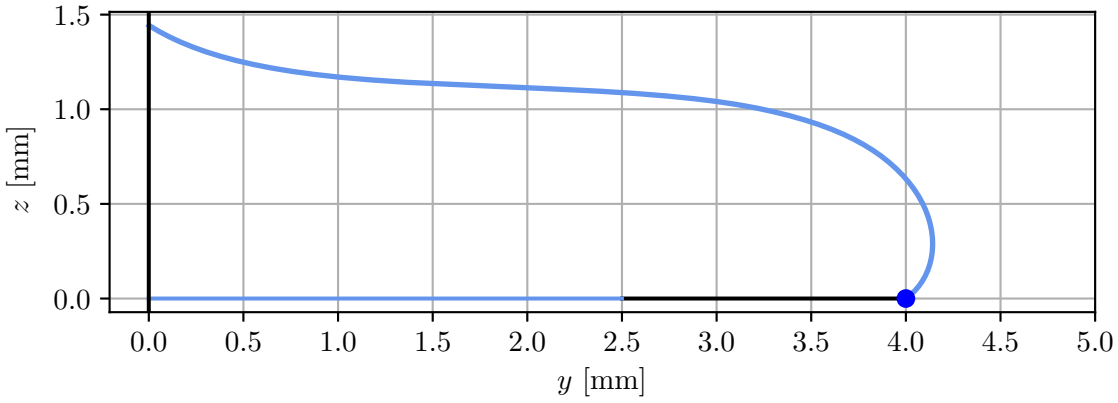

(a) $\theta = 68°$.

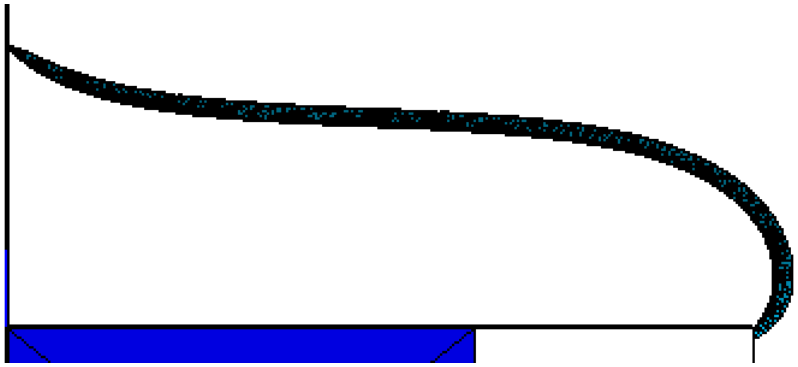

(b) $\theta = 68°$.

Figure 4.8: Shape of the interface water-air obtained from the numerical resolution of the analytical problem constraint by the boundary set 2 compared with the shape of the interface obtained by surface Evolver. The different parameters are $H_z = 1.5$ mm, $W_{tot} = 4$ mm, $t = 1$ mm, $g_{art} = 210$ m/s^2 and $\theta = 68°$.

In a quantitative way, the volume and total energy related to body 2 can be computed for both models. The energies associated with both shapes are obtained with $\theta = 68°$. From these parameters the volume and energy of both models can be computed and the results are shown

in Tab.4.1.

	Volume mm	Total energy μJ
Analytical model	4.450	2.192
Surface Evolver model	4.433	2.279
Difference	0.017	0.088
Relative difference %	0.38	3.82

Table 4.1: Volumes and energies obtained with the analytical and SE model for $H_z = 1.5$ mm, $W_{tot} = 4$ mm, $t = 1$ mm, $g_{art} = 210$ m/s^2, $\theta = 68°$. The relative difference has been computed with respect to the Surface Evolver model.

It can therefore be concluded that the predictions of the two models are very close to each other, in terms of the shape of the interface as well as in terms of total energy and volume associated. Moreover, the difference in energy can be explained by the fact that some of the edges of the Surface Evolver model have already begun to move along the vertical plane of the inter-chamber, increasing the surface energy.

CHAPTER 5

SENSITIVITY ANALYSIS

In this chapter, the sensitivity of the volume in the metering chamber with respect to the different parameters introduced in Ch. 2 is studied. Firstly, using Surface Evolve, a way to determine the volume in the metering chamber just before the fluid overflows into the waste chamber is established. Then, this method is applied to the analytical model and the sensitivity study method is described. After that, the results obtained with the analytical model are presented and discussed. Finally, some results obtained with the SE model are compared with the one of the analytical model.

5.1 Determination of the critical volume

In order to study the sensitivity of the volume of body 2 just when the fluid begins to flows in the waste chamber, a way to compute this volume must be found. This volume will be called critical volume and must be determined in different ways depending on the model used. However, both relate to the contact angle made by the liquid and the right edge of the inter-chamber just before the liquid flows into the second chamber, this contact angle will be called critical contact angle θ_{crit}.

5.1.1 Physics on the edge

When the volume of liquid of body 2 increases, the triple line between the inter-chamber and the liquid moves towards the right edge of the inter-chamber with an advancing contact angle θ_{a} due to contact angle hysteresis, as explained in Sec. 1.1.7. Once the triple line has reached the edge, it stays pinned on the corner until the critical angle θ_{crit} is bigger than a certain limit $\alpha+\theta$ where $\alpha = 90°$ is the angle between the horizontal and vertical wall of the inter-chamber. Once this limit has been reached, the fluid begins to move along the vertical wall of the inter-chamber, as shown in Fig.5.1.

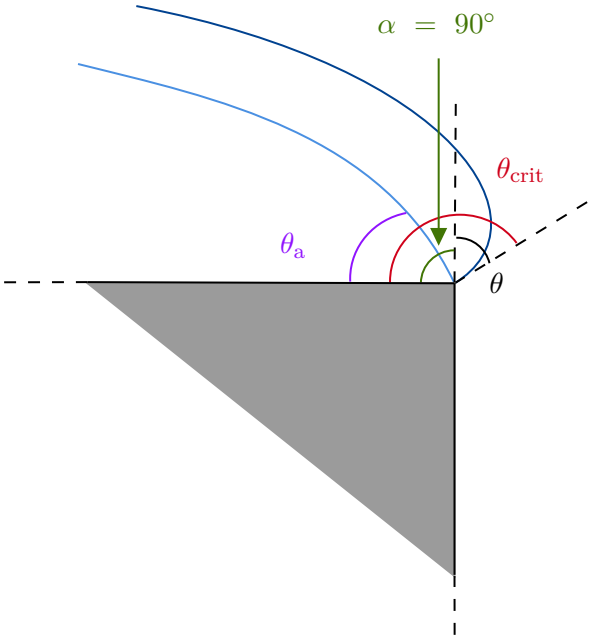

Figure 5.1: Evolution of the interface on the edge of the inter-chamber. θ_a is the contact angle between the solid and the fluid when the volume of the fluid increases, α the angle made by the two planes of the corner, θ the Young contact angle and θ_{crit} the angle at which the liquid begins to move on the vertical plane.

The first step to determine the critical volume is then to know if the liquid begins to flow at constant volume into the waste chamber when its contact angle has reached the critical contact angle, i.e, begins to flow along the vertical wall, or not. If it does, the critical volume could then be determined by computing the volume associated with the interface making a contact angle θ_{crit} with the edge. As the analytical model can not simulate the transition on the edge and an iterative augmentation of the volume, it will be explored by using Surface Evolver.

5.1.2 SE model

Fluid evolution

Thanks to the constraints defined in Sec. 4.3.3, a script that transfers the triple line from the horizontal to the vertical plane of the inter-chamber can be built. The script works as follows:

1. The liquid evolves toward the edge.
2. Once the triple line has reached the edge, the volume of the liquid is increased iteratively and at each iteration the angle between the normal of the different facets that have an edge on the corner and the horizontal plane is computed. This angle corresponds to $\theta_{edge} + 90°$, where θ_{edge} is the contact angle on the edge between the horizontal plane and the liquid.
3. When this angle is bigger than a certain threshold θ_{tresh}, defined as

$$\theta_{tresh} = \frac{\theta + (\theta + 90)}{2},$$

the constraints maintaining the edges on the horizontal plane are replaced by constraints maintaining the edge on the vertical plane. This allows the edges to move along the vertical plane if it reduces the surface energy of body 2.

4. The volume keeps increasing, at a certain point all the edges on the triple line will be free to move on the vertical plane.

5. Once all the edges have been transferred, the volume is increased until all the edges have begun to move along the vertical plane.

6. When all the edges begin to move on the vertical plane, the volume stops increasing and Surface Evolver runs gradient descent iterations at constant volume.

At this point, if the liquid flows along the vertical plane of the inter-chamber towards the bottom of the waste chamber while maintaining a constant volume, it can be concluded that the critical volume is the one obtained when all the edges begin to move on the vertical wall and the question asked in the previous subsection is answered.

Results

This evolution of the body 2 during the script is then illustrated in Fig.5.2. When all the edges begin to move on the vertical plane of the inter-chamber and Surface Evolver runs gradient descent iterations at constant volume, as in Fig. 5.2d, it can be seen that the fluid flows toward the bottom of the waste chamber. This result answers the question raised there above, since the fluid flows at constant volume in the waste chamber once it is allowed to move along the vertical plane, the critical volume can be defined by the volume under the interface making a contact angle θ_{crit} with the corner.

This result is especially important for the analytical model. As this model cannot simulate an iterative increase of the volume or a transfer on the vertical wall of the inter-chamber, the critical volume will only be determined by the volume related to the interface making a contact angle θ_{crit} with the corner.

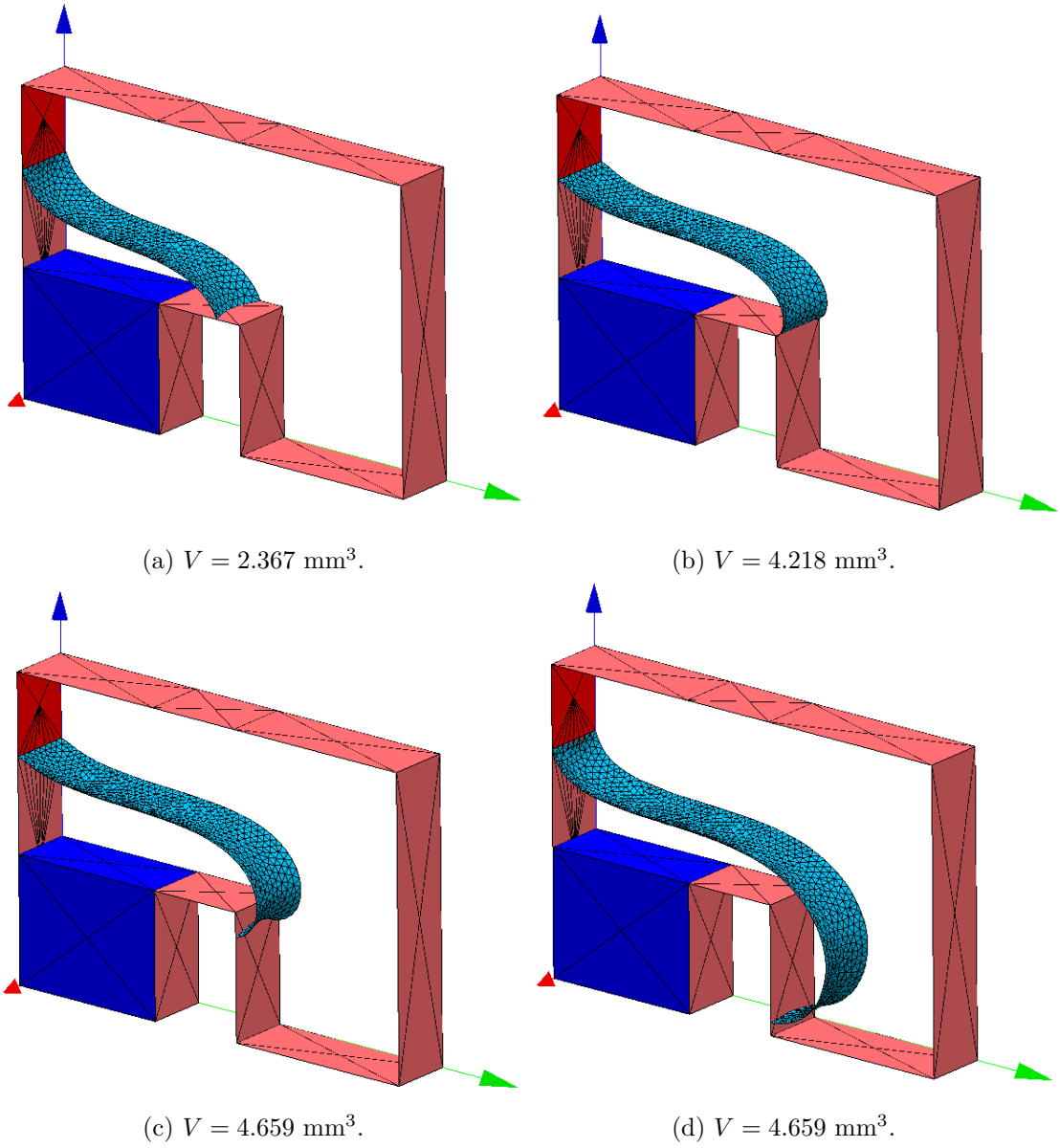

(a) $V = 2.367$ mm^3.

(b) $V = 4.218$ mm^3.

(c) $V = 4.659$ mm^3.

(d) $V = 4.659$ mm^3.

Figure 5.2: Evolution of the fluid as described in Sec. 5.1.2. 5.2a the fluid moves toward the right edge of the inter-chamber. 5.2b the fluid has reached the corner and all the edges have been transferred to the vertical wall. 5.2c All the edges have started to move along the vertical wall and the volume stops increasing. 5.2c Several gradient descent iterations are run at constant volume. The parameters are $H_z = 1.5$ mm, $W_{tot} = 4$ mm, $t = 1$ mm, $g_{art} = 210$ m/s^2 and $\theta = 68°$.

Moreover, it is interesting to look at the evolution of the fluid in thicker operation units, as illustrated in Fig. 5.3. It can be seen that due to the curvature of the interface in the depth of the operation unit, coming from the equivalent centrifugal pressure presented in Sec. 1.2.2, the edges close to the back and front plane of the LoD reach the corner before the one in the centre. Since the edges on the sides reach the corner earlier, they are also transferred to the vertical wall before the edges in the centre, and therefore they begin to move toward the bottom of the edge first. This phenomenon is also present on a much smaller scale in Fig. 5.2 but is highlighted when the thickness of the operation unit is increased as it leads to a bigger curvature in the

depth of the chambers.

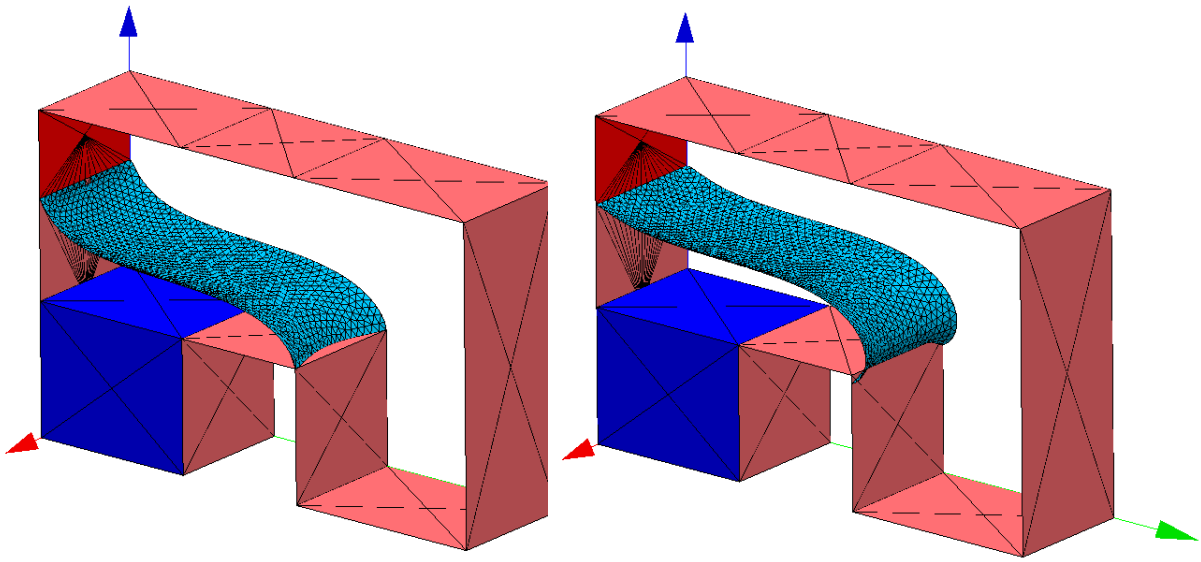

(a) The edges on the sides have reached the corner.

(b) The edges on the sides begin to move on the vertical plane.

Figure 5.3: Evolution of the fluid for $H_z = 1.5$ mm, $W_{tot} = 4$ mm, $t = 2$ mm, $g_{art} = 210$ and $\theta = 68°$.

Finally, the contact angle between the vertical wall and the liquid when it flows into the waste chamber should be equal to the Young-Dupré contact angle θ, as explained in Sec .1.1.7. However, it has been observed in the Surface Evolver model that the contact angle is in fact lower than the Young-Dupré contact angle. This phenomenon has been observed by the Uliege Microfluidic lab in other geometries. In fact, at fixed surface energies, the minimum energy forms do not necessarily correspond to the Young-Dupré contact angle but are sometimes smaller. It can be observed in the case of a pendent drop when gravity resists the surface tension. It means that the system allows itself lower contact angles than chemically expected if this allows it to further reduce its potential energy. It is clearly a similar case to the one studied here so it looks like Surface Evolver finds this minimum energy solution, and not the one with a fixed contact angle.

5.1.3 Analytical model

As explained earlier, since the analytical model solves the mathematical equations describing the shape of the interface for precise initial conditions corresponding to the pinning on the edge of the inter-chamber, it cannot iteratively increase the volume of the liquid or transfer the liquid from one wall to the other. Therefore, the ODE system is solved with initial conditions corresponding to a pinning on the corner of the inter-chamber with a contact angle θ_{crit}. The shape of the interface, just when it starts to move along the vertical plane and flows at constant volume into the waste chamber, is therefore obtained. Finally, the volume of this shape is computed as explained in Sec 3.3, which corresponds to the critical volume.

5.2 Sensitivity study method

Now than the critical volume can be obtained easily for each parameter configuration and that the different dimensionless parameters of interest have been established, a method to study the sensitivity of the critical volume to variations of the parameters must be defined. The idea is then to choose a set of 3 different values of interest for each dimensionless number and to vary the numbers around these three values. For each combination of parameters, the associated critical volume is computed. Finally, the evolution of the critical volume around the different sets of parameters can be obtained.

However, the Surface Evolver model is not able to run automatically several simulations with different parameters. The analytical model will therefore be used to explore the whole sets of combinations of parameters and the results will be compared with the one of SE for some well-chosen set of parameters.

5.2.1 Choice of the parameter's value

As the length W_{tot} has been chosen as the denominator of most of the dimensionless parameters, it will stay constant and equal to 4 mm along the study.

Moreover, the relation between the thickness t of the LoD and the volume under the interface in the analytical model is linear as the volume is expressed by Eq. 3.3. The volume is therefore simply directly proportional to the thickness of the operation unit, as shown in Fig. 5.4, and the influence of π_4 does not need any in depth study here. However, it has a different impact when the curvature along the depth of the chambers is taken into account, as in the SE model. The influence of this parameter on the critical volume will therefore be studied in Sec. 5.4.

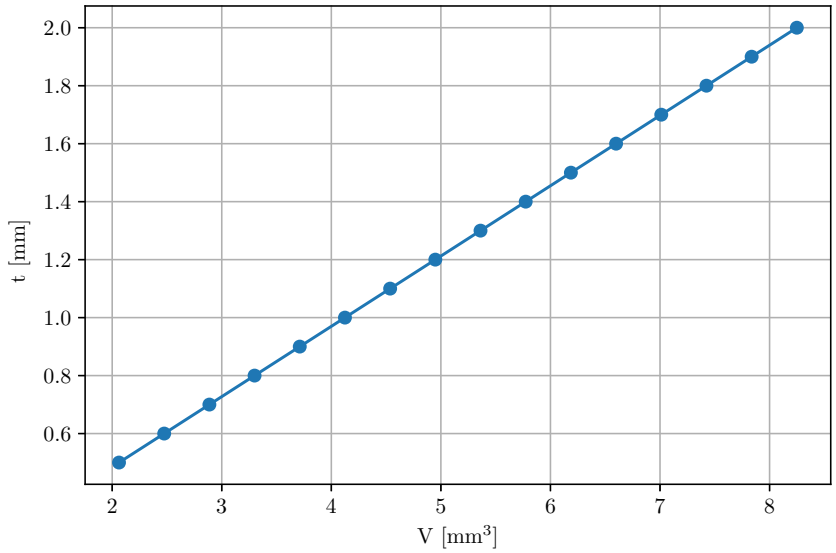

Figure 5.4: Evolution of the critical volume obtained through the analytical model with respect to the thickness t of the operation unit. The parameter are $H_z = 1.45$ mm, $W_{\text{tot}} = 4$ mm, $\theta = 68°$, $g_{\text{art}} = 210$ m/s^2.

After that, the parameters left are H_z, λ_c and θ, each one involved respectively in π_1, π_2 and π_3. The goal is to define a three-dimensional phase space and to choose three values for each parameter around which the sensitivity of the critical volume will be quantified. Proceeding this way, the sensitivity will be studied in each region of the phase space.

Firstly, the 3 values chosen for H_z are 0.8 mm, 1.2mm and 1.6mm, each one corresponding to a realistic height of pinning of the liquid. This leads to the three points $\pi_1 = 0.2$, $\pi_1 = 0.3$ and $\pi_1 = 0.4$ in the space of dimensionless numbers.

Secondly, the only parameter in λ_c that can vary during the experiment is g_{art}. The first value of this parameter has been chosen to $g_{\text{art}} = 50$ m/s^2 so that the rotation per minute needed to achieve this artificial gravity is of $N = 389.85$ RPM. This corresponds to a capillary length of $\lambda_c = 1.202$ mm, leading to a rounded meniscus, as it has been shown in Sec. 4.5.1. The second value is $g_{\text{art}} = 200$ m/s^2 corresponding to $N = 779.70$ RPM and $\lambda_c = 0.6$ mm, which is close to the rotational speed used in the latest experiments made by the Microfluidic lab. Finally, $g_{\text{art}} = 350$ m/s^2 is chosen as the last value of this range, it corresponds to $N = 1031.44$ RPM and $\lambda_c = 4.542$ mm. This value has been chosen to have a more flattened meniscus, as in Sec. 4.5.1. The three values of π_2 associated to those 3 capillary length are $\pi_2 = 0.30$, $\pi_2 = 0.15$ and $\pi_2 = 0.11$.

Finally, the values of $\pi_3 = \theta$ have been chosen equal to 50°, 65°, 80°, so that different levels of hydrophilicity are studied. The different parameter values are summarised Tab. 5.1

π_1	H_z	π_2	g_{art}	$\pi_3 = \theta$
0.2	0.8	0.30	50	50
0.3	1.2	0.15	200	65
0.4	1.6	0.11	350	80

Table 5.1: Values around which the phase space will be explored.

Therefore, 27 regions of the phase space will be explored. For each region, the variation of the volume with respect to the variation of one parameter around its central value will be studied, resulting in 81 sensitivity coefficients. The central values will correspond to the centre of the region, given here above.

5.2.2 Sensitivity quantification

In order to study the impact of each parameter on the sensitivity of the critical volume, the range of variation $\Delta\pi$ [−] of each parameter around its central value π_{ce} [−] will be of ±1%. The central values correspond to the values in Tab. 5.1. Given that the variation is infinitesimal, this guarantees that the relationship between the critical volume and the variation in the parameter is linear. This is illustrated in Fig.5.5

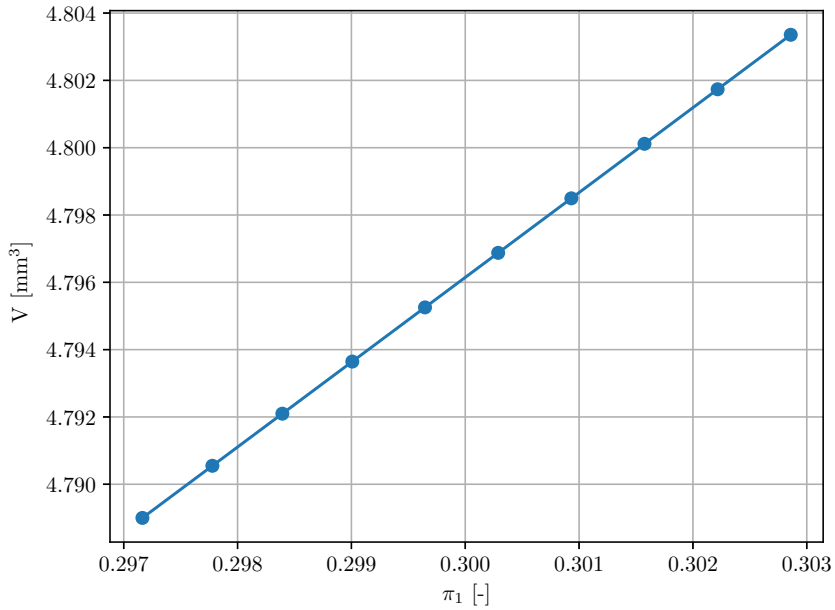

Figure 5.5: Evolution of the critical volume around $\pi_1 = 0.3 \pm 1\%$. The parameter are $H_z = 1.2$ mm, $W_{tot} = 4$ mm, $\theta = 60°$, $g_{art} = 200$ m/s^2.

After that, a first-order polynomial fitting can be made in order to determine a linear function $V_{crit}(\pi)$, establishing a link between the varying parameter and the critical volume. The first-order derivative of this function can then be computed in order to get the slope ΔV_{crit} [mm^3] of the function and quantify the variation of the critical volume with respect to a variation of the parameter studied. Once ΔV_{crit} has been computed, the relative variation $\Delta V_{crit}/V_{crit,\,ce}$ of the critical volume with respect to the infinitesimal variation of $\pm 1\%$ of the parameter can be obtained as

$$S_\pi = \frac{\Delta V_{crit}/V_{crit,\,ce}}{\Delta\pi/\pi_{ce}},$$

where S_π $[-]$ is the sensitivity coefficient of the critical volume with respect to a variation of $\pm 1\%$ of π and $V_{crit,\,ce}$ is the critical volume obtained with the central value π_{ce} of the studied range. The value of S_π indicates therefore by which percentage the critical volume changes when π changes of $\pm 1\%$.

5.3 Results with the analytical model

Now that the sensitivity study method has been established, the different sensitivity coefficients obtained with the analytical model are presented in Fig. 5.6. Moreover, all the sensitivity coefficients have been reported in Tab. A.1, Tab. A.2 and Tab. A.3 in the appendix. The minimum and maximum sensitivity coefficients, as well as the median coefficients, have been computed in order to compare the impact of the different parameters on the critical volume sensitivity.

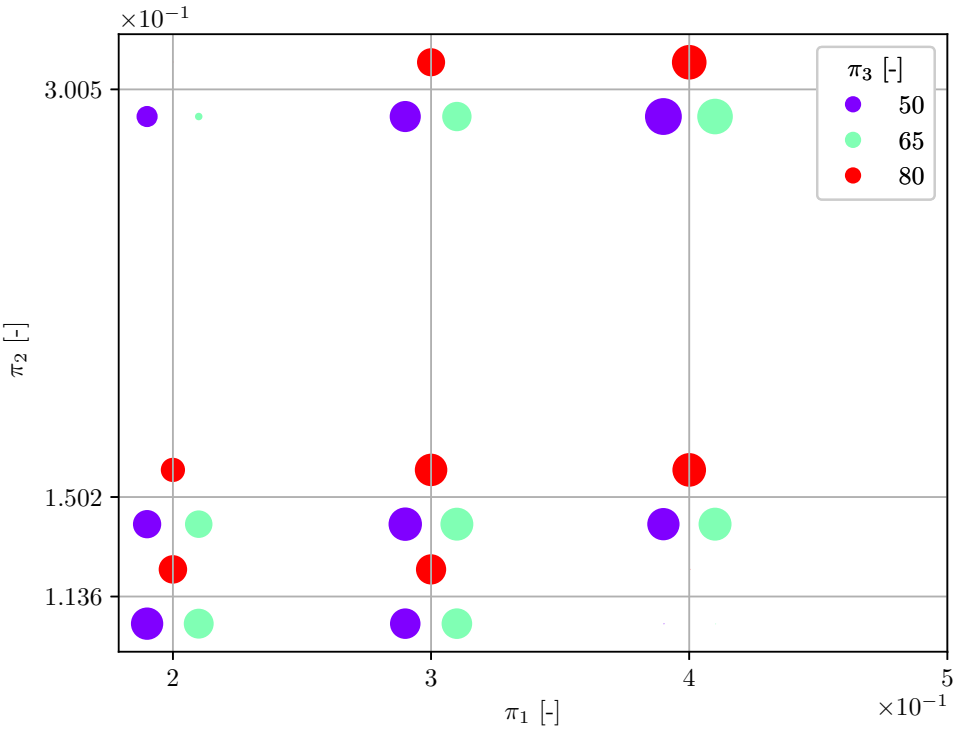

(a) Coefficient with respect to a variation of π_1. $S_{\pi_1,\max} = 0.22$, $S_{\pi_1,\min} = 0.003\%$, $S_{\pi_1,\text{median}} = 0.13$

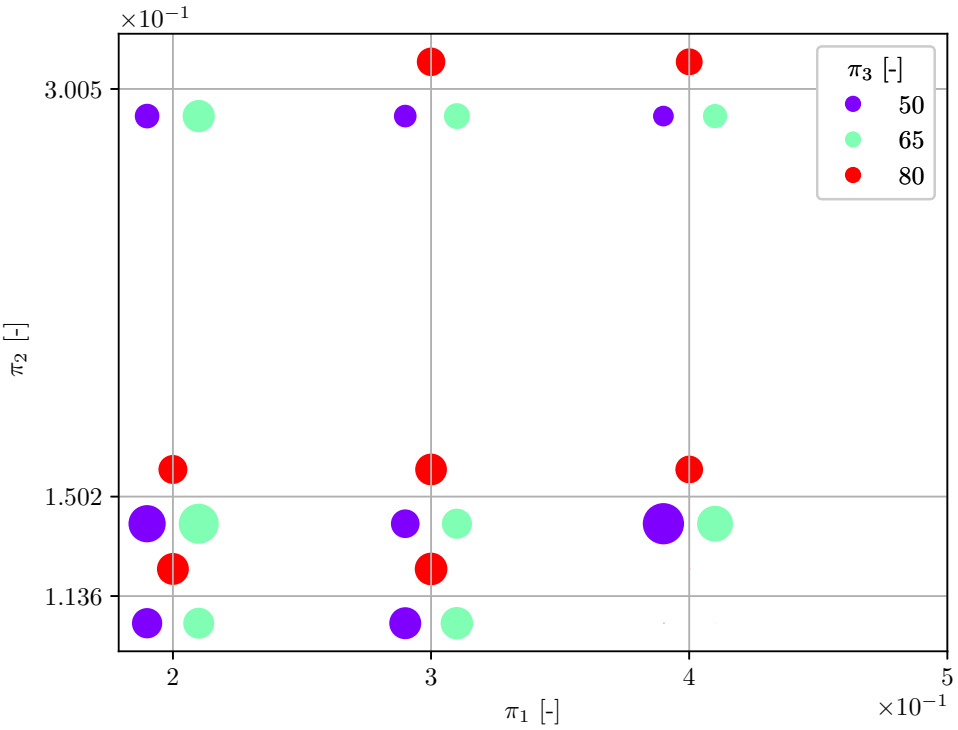

(b) Coefficient with respect to a variation of π_2. $S_{\pi_2,\max} = 1.28$, $S_{\pi_2,\min} = 0.62$, $S_{\pi_2,\text{median}} = 0.81$

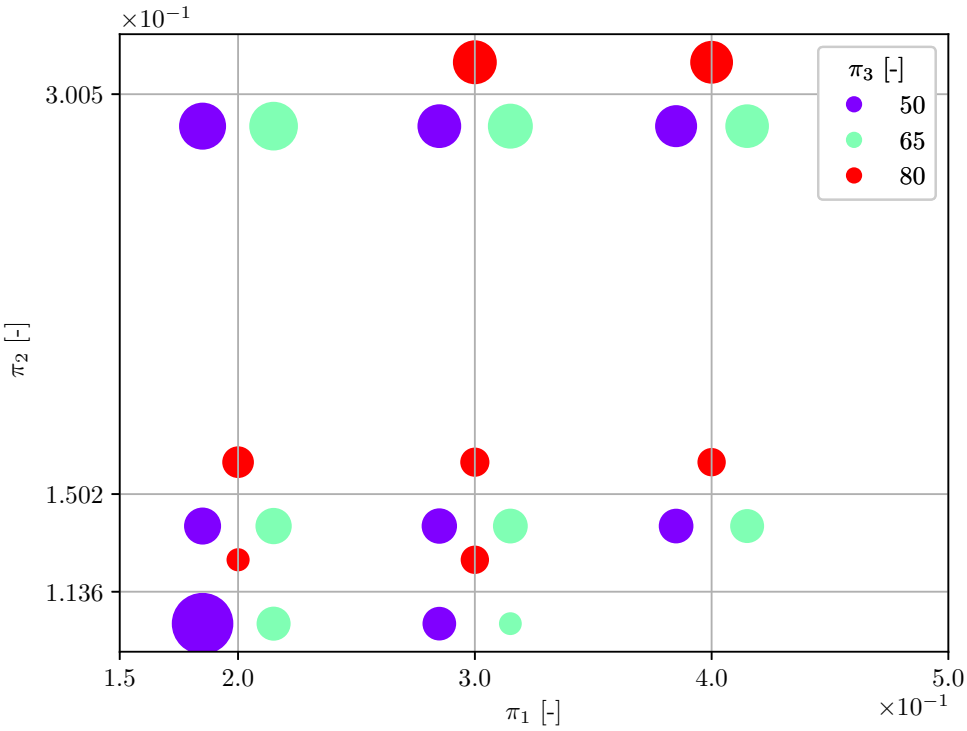

(c) Coefficient with respect to a variation of π_3. $S_{\pi_3,\max} = 0.88$, $S_{\pi_3,\min} = 0.04$, $S_{\pi_3,\text{median}} = 0.2$

Figure 5.6: Representation of the 3D phase coefficient projected in the 2D π_1 - π_2 plane, while the colour of the dots indicates the corresponding π_3. The size of the dots represents the relative value of the sensitivity coefficients. The size of the coefficient on two different graphs cannot be compared. In fact, the coefficients have undergone linear combinations of logarithms to highlight their difference on the same graph. However, the smallest and largest coefficient, as well as the median of the coefficients, are specified in the sub-caption in order to compare the overall impact of a dimensionless number with respect to the other.

5.3.1 Discussion

In general, it can be seen in the graphs that there exist no solutions for some regions of the phase space, meaning that the κ satisfying the boundary conditions imposed by the region has not been found. Firstly, the combination $\pi_1 = 0.2$, $\pi_2 = 0.30$ and $\pi_3 = 80$ ($H_z = 0.8$ mm, $g_{\text{art}} = 50$ m/s^2 and $\theta = 80°$) seems not to present any solution. It could come from the fact that the water should have already overflown if it has met this set of conditions. The same phenomena can be observed for all contact angles associated with $\pi_1 = 0.4$ and $\pi_2 = 0.11$ ($H_z = 1.6$ mm and $g_{\text{art}} = 350$ m/s^2), which could mean that a pinning on the left wall at these heights is impossible for such artificial gravity, or that for the three contact angles of the phase space a fluid pinned at this height and submitted to this artificial gravity should have already flown into the waste chamber.

Also, higher artificial gravity than $g_{\text{art}} = 350$ m/s^2 could not be explored using the analytical model. In fact, as g_{art} increases the range of kappa that respect the boundary condition $y(s =$

max) is smaller and smaller and no kappa respecting the boundary condition $z(s = \max) = H_z = 0.8$ mm, 1.2 mm or 1.6 mm could be found. The sensitivity for higher rotation speed will therefore be explored using the Surface Evolver program.

Impact of π_1

First of all, based on the median sensitivities, it can be concluded that with $S_{\pi_1,\text{median}} = 0.13$ the first dimensionless parameter is the one that has the least impact on the critical volume sensitivity. This is fortunate as this dimensionless number depends on two geometrical parameters, each one submitted to manufacturing tolerances.

Moreover, the region where the critical volume is the least sensitive to a variation of π_1 is where $H_z = 0.8$ mm and $g_{\text{art}} = 50$ m/s^2, furthermore, the sensitivity is especially low for $\pi_3 = \theta = 65°$. In general, it can be noticed that the sensitivity is slightly lower at $\pi_1 = 0.2$ than at other values of π_1. It could come from the fact that since the pinning is lower, the relative variation of $\pm 1\%$ of $\pi_1 = 0.2$ corresponds to a lower variation than for $\pi_1 = 0.4$ mm, leading to lower relative variations in the volume.

Finally, the sensitivity is the biggest in the region $\pi_1 = 0.4$ and $\pi_2 = 0.30$, and so for each value of π_3. It could be explained by the fact that as the artificial gravity is lowered the capillary number λ_c increases, meaning that the capillary force takes more and more the lead over body forces. This results in stronger capillary forces and more rounded meniscus, so that the liquid tends to evolve more vertically before flowing into the waste chamber. However, as the pinning on the left wall increases, this rounded shape is more and more pushed to the corner, so a slight increase of the pinning height could have a big influence on the critical volume.

Impact of π_2

First of all, based on the median sensitivities it is clear that with $S_{\pi_2,\text{median}} = 0.81$ it is the parameter π_2 that has the biggest impact on the critical volume sensitivity. Moreover, this median is way above the median $S_{\pi_1,\text{median}} = 0.13$ and $S_{\pi_3,\text{median}} = 0.18$ of the two other parameters and so this parameter is particularly distinct from the other two. In extension, it means that it is the artificial gravity induced by the rotation of the LoD that plays the biggest role in the sensitivity of the volume before the overflow. This result should be appreciated by the experimenters as they have the entire control over this parameter and it stays constant during the metering process.

Moreover, as this dimensionless number is inversely proportional to the artificial gravity, positive sensitivity coefficients mean that the critical volume increases as g_{art} decreases. This result could be expected, as when the gravity is lowered the capillary number λ_c increases, meaning that the capillary force takes more and more the lead on body forces. As explained above, the liquid tends therefore to evolve more vertically before flowing into the waste chamber. Shapes for lower artificial gravity have been shown in Sec. 4.5.1.

By analysing Fig. 5.6b in detail, it can be seen that the sensitivity at $\pi_2 = 0.30$, or $g_{\text{art}} = 350$, m/s^2 is on average lower than the sensitivity in the two other regions of π_2, meaning that the critical volume is less sensitive to variation of the artificial gravity when it is high. However, the region where the volume is the most sensitive in average is for $\pi_2 = 0.15$. This makes sense as it is the region where the capillary and body forces are the most in balance with each other so a small variation of one of the two forces could lead to a disequilibrium in this balance.

Impact of π_3

Fristly, $\pi_3 = \theta = 80°$ is the contact angle that presents on average the least sensitivity. It means that at this contact angle at the edge, the shape of the interface is not highly influenced by a variation of the contact angle and it will be overall the same shape for any contact angle around $\theta = 80°$.

Moreover, the critical volume is more sensitive to variation in the contact angle at low artificial gravities. This could be explained by the fact that, as said above, at this capillary number the meniscus is rounded. Therefore, a variation in the contact angle at the edge influences a lot the rounded shape of the meniscus, leading to significantly different volumes even for small variations in the contact angle.

Finally, it can be noticed that the maximum sensitivity is reached at $g_{\text{art}} = 350$ m/s^2, $z = 0.8$ mm and $\theta = 50°$.

5.4 Results with the SE model

As the impact of the different parameters has been studied using the analytical model, the different results discussed here above will be compared with Surface Evolver results. Moreover, the study of the depth t [mm] of the operation unit will be explored through the dimensionless number $\pi_4 = t/W_{\text{tot}}$. Finally, the sensitivity for higher artificial gravity will be explored.

First of all, the sensitivity coefficients of π_1, π_2 and π_3 at the central region $\pi_{1,\text{c}} = 0.3$, $\pi_{2,\text{c}} = 0.15$ and $\pi_{3,\text{c}} = 65°$ have been computed using Surface Evolver. It results in $S_{\pi_1} = 0.25$, $S_{\pi_2} = 0.82$ and $S_{\pi_3} = 0.42$.

After that, the sensitivity of the critical volume with respect to variations of the depth t [mm] around $\pi_{4,\text{c}} = 0.125$, $\pi_{4,\text{c}} = 0.250$ and $\pi_{4,\text{c}} = 0.375$, corresponding to $t = 0.5$ mm, 1 mm and 1.5 mm has been computed at the region $\pi_1 = 0.3$, $\pi_2 = 0.15$ and $\pi_3 = 65°$. The simulations produced with Surface Evolver gave $S_{\pi_4=0.125} = 0.9$, $S_{\pi_4=0.250} = 0.87$ and $S_{\pi_4=0.375} = 0.92$.

Finally, the sensitivity of the volume with respect to variations of π_2 at high artificial gravity $g_{\text{art}} = 700$ m/s^2, corresponding to $\pi_{2,\text{c}} = 0.80$, has been studied. This sensitivity computation has been made in the region corresponding to $H_z = 0.4$ mm, $\theta = 65°$ and $t = 1$ mm. The

pinning has been chosen much lower than for other sensitivity studies as the analytical model showed that at such an artificial gravity no solutions could be found for pinning higher than $H_z = 0.55$ mm. It results in a sensitivity coefficient of $S_{\pi_2} = 1.43$. Moreover, shape of the interface obtained at $g_{\text{art}} = 700$ m/s^2 is represented in Fig. 5.7.

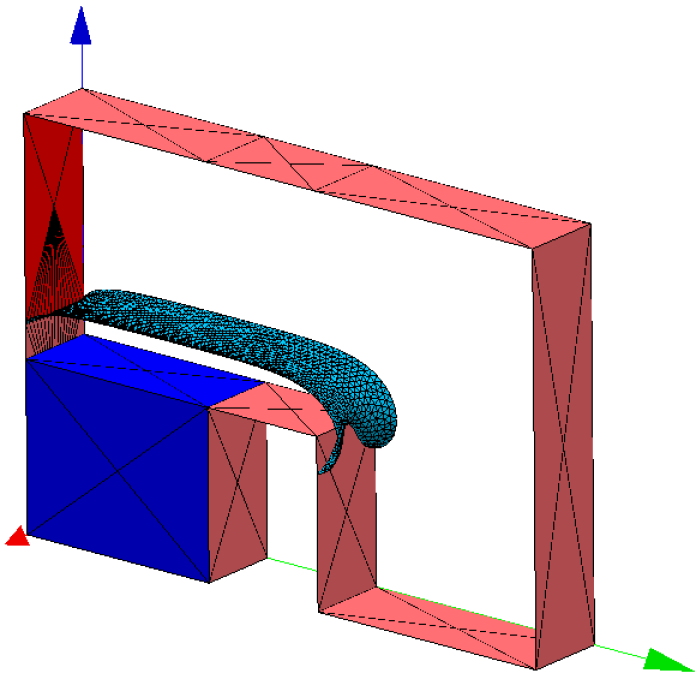

Figure 5.7: Shape of the interface just when the fluid begins to flow into the waste chamber. $W_{\text{tot}} = 4$ mm, $H_{\text{z}} = 0.4$ mm, $t = 1$ mm, $g_{\text{art}} = 700$ m/s^2 and $\theta = 65°$.

5.4.1 Discussion

Firstly, the sensitivity $S_{\pi_1} = 0.25$ obtained with $\pi_{1,\text{c}} = 0.3$, $\pi_2 = 0.15$ and $\pi_3 = 65°$ on Surface Evolver is higher that the maximal sensitivity $S_{\pi_1,\text{max}} = 0.22$ obtained with the analytical model. It means the curvature induced by the equivalent centrifugal pressure along the depth t [mm] of the operation unit tends to increase the sensitivity of the critical volume to the height of the pinning on the left wall. Moreover, for the same conditions, the sensitivity coefficient $S_{\pi_3} = 0.42$ obtained through the Surface Evolver model is bigger than the one of 0.19 obtained with the analytical mode at the same region. This result makes sense as the contact angle plays a bigger role in the SE model. In addition to determining the angle at which the liquid begins to overflow in the waste chamber, as in the analytical model, it also plays a role in the curvature of the meniscus along the depth of the LoD, which has an influence on the total volume of the liquid.

However, this phenomenon is not observed for π_2, where the sensitivity $S_{\pi_2} = 0.82$ of the SE model is really close to the one of 0.81 obtained with the help of the analytical model with the same other parameters. This result is counter-intuitive as artificial gravity plays a major role in the equivalent centrifugal pressure, leading, as explained above, to a bending of the meniscus in the depth of the metering operation unit. On the other hand, it could mean that the capillary and body forces are in a balance such that even if the artificial gravity tends to vary a little,

the capillary forces remain dominant and control the depth bending. This hypothesis is corroborated by the last result, highlighting the impact of the contact angle on the perpendicular bending.

After that, it is interesting to analyse the results of the sensitivity study of $\pi_4 = t/W_{tot}$. The different sensitivity coefficients $S_{\pi_4=0.125} = 0.9$, $S_{\pi_4=0.250} = 0.87$ and $S_{\pi_4=0.375} = 0.92$ are indeed pretty high with respect to those of the other three dimensionless parameters. It could be expected as the thickness of the LoD directly impacts the quantity of volume allowed in the metering operation unit.

Finally, the sensitivity of the critical volume with respect to variation of high artificial gravity must be discussed. The obtained sensitivity coefficient $S_{\pi_2} = 1.43$ shows that the critical volume is quite sensitive to variation of high g_{art}. It demonstrates that at high sensitivity, the perpendicular bending of the meniscus is more dependent on the equivalent centrifugal pressure induced by the rotation of the LoD than for lower artificial gravity. At these numbers, the balance between the capillary and the body force is therefore dominated by the second one. However, as said in the discussion of the results obtained with the analytical model, the artificial gravity can be chosen to be exactly the same during different experiments, so that no change of critical volume due to variation of the artificial gravity is expected between two different processes.

5.5 Short conclusion

First, it must be noted that the majority of coefficients are around $S_\pi = 1$, indicating some proportionality between the volume and the associated π. This is fortunate as high sensitivity, for example of $S_\pi = 10$, would really be problematic because it would be impossible to meter the liquid sample properly without having a perfect control on the corresponding π.

Moreover, the experiments used to design the metering chambers with respect to a specific rotational speed, which must also be convenient for the different microfluidic valves around the operation unit. After that, when the experiments are done, it could happen that the speed of rotation chosen before the chip is manufactured is not optimal. The results presented here above shows that the selected volume could also be modified by the rotational speed, something that has never been taken into account by the experimenters before.

CHAPTER 6

IMPACT OF TOP WALL

In this chapter, the effect of the relative height of the top wall of the metering chamber with respect to the inter-chamber is studied. First, the impact of this top wall on the problem is explained and the physics behind the introduced phenomenon is described. Then, the way the analytical model is adapted in order to introduce and study the effect of the top wall is established. Finally, the results obtained with the model are presented and discussed.

6.1 Impact of the top wall on the problem

As mentioned in Sec.2.3, the parameter H_{up} corresponds to the relative height of the top wall of the chamber with respect to the inter-chamber and plays an important role in the shape of the interface before the overflow. In fact, depending on the process history the interface could, or could not, be attached to the top wall before it flows into the waste chamber. This top connection depends on the position of this wall with respect to the inter-chamber as well as the way the chamber is filled.

Furthermore, in some different metering operation units, top pinning is required by the experimenters. Metering operation units where top pinning is unavoidable and is an integrated part of the metering process are shown in Fig. 6.1. It is therefore interesting to study at which position the top wall should be so that the liquid is attached to it

6.2 Physics behind the top wall attachment

One can imagine the case of a droplet squeezed between two horizontal walls. If the top wall is moving up there will come a time when the drop will come of the top wall and just lie on the bottom plane. This change of shapes comes from the fact that the attachment to the top wall does not correspond to the shape of minimal energy and the contact angles between the top walls and the liquid are not feasible anymore. This phenomenon is illustrated in Fig.6.2.

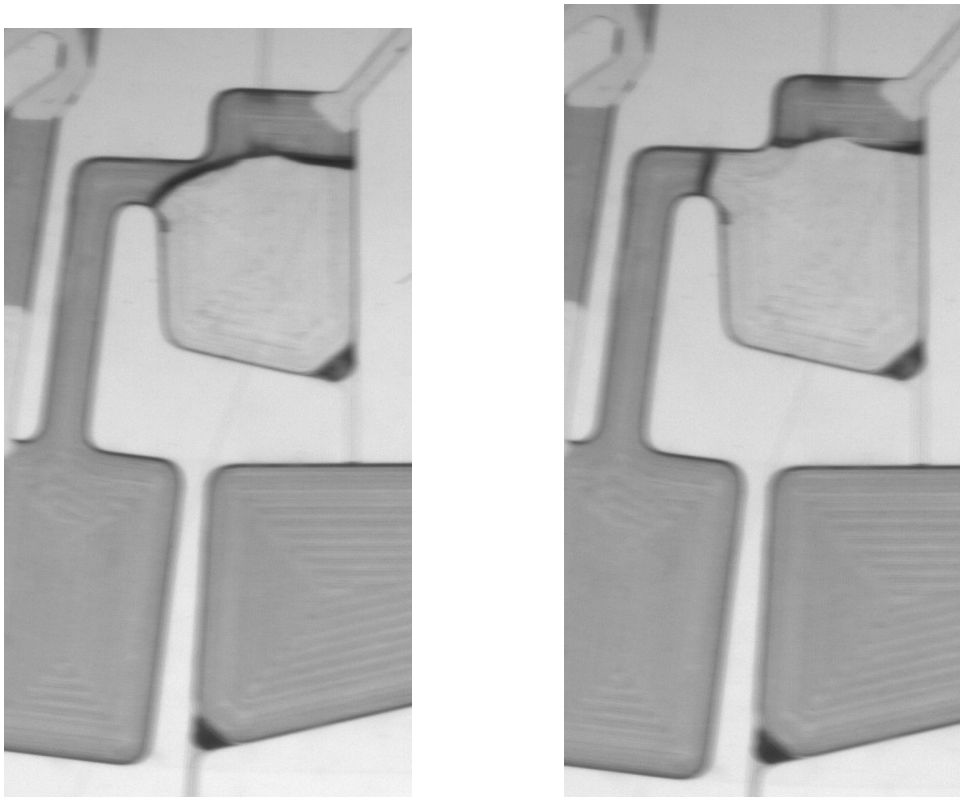

(a) One frame before the liquid connects with the top wall.

(b) One frame after the liquid connects with the top wall.

Figure 6.1: Front view of a metering operation unit where an attachment to the top wall is unavoidable and part of the process.

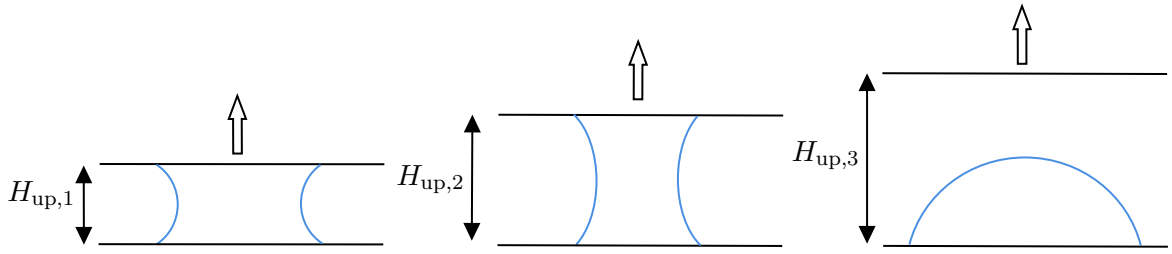

Figure 6.2: The blue curves defined the shape of the interface liquid-air, the black straight lines define the bottom and top planes between which the droplet is initially squeezed, H_{up} is the distance between the two planes. The arrow indicates the direction of the top wall. The initial state is on the right and the final is on the left.

However, if the droplet lies on the bottom wall and the top wall is being brought closer and closer to the droplet, the liquid will end up attaching itself to the top wall when it comes into contact with the drop.

From these two cases, a range of H_{up} where the drop could either be attached to the top wall or lying on the bottom plane could be established. The upper limit is defined by the height $H_{up,high}$ at which the initially squeezed liquid would detach from the top wall. The lower limit $H_{up,low}$ corresponds to the highest point of the interface itself when the liquid is initially lying

on the bottom plane. For each height H_{up} in this range two corresponding interfaces could be associated, one attached on the top plane and another one lying on the bottom plane, each one corresponding to different surface energies. This range corresponds to a meta-stable region and the actual shape of the interface will then depend on the past of the system.

If this principle is applied to the problem of this master thesis, the lower limit will be the same but the definition of the upper limit should be slightly modified. The upper limit is in this case defined by the height at which the initially squeezed liquid would detach itself from the top wall to attach itself to the left wall.

Moreover, the shape of the interface, and therefore the upper and lower limit of the range, depends on the contact angle between the liquid and the solid surface. The evolution of this range with respect to the contact angle θ should therefore be studied.

6.3 Implementation in the analytical model

6.3.1 Top wall attachment

The equations and method of resolution remain the same as those presented in Ch.3. However, a supplementary boundary condition is added to the problem. This boundary condition includes the top wall of the inter chamber, situated at H_{up}, and is defined as in Tab. 6.1.

	$y(s_{\max})$	$z(s_{\max})$	$\varphi(s_{\max})$
	m	m	–
Boundary conditions 3	Free	H_{up}	θ_{top}

Table 6.1: Sets of boundary conditions corresponding to an attachment on the top wall. H_{up} represents the distance between the inter-chamber and the top wall and θ_{top} corresponds to the contact angle between the liquid and the top wall.

In other words, the equations defining the shape of the liquid-air interface will be solved for a series of different κ, and then the shape which respects the boundary conditions 3 will be selected, i.e an attachment to the top wall with a contact angle of $\theta_{\text{top}} = \theta$. It results in shapes like in Fig. 6.3.

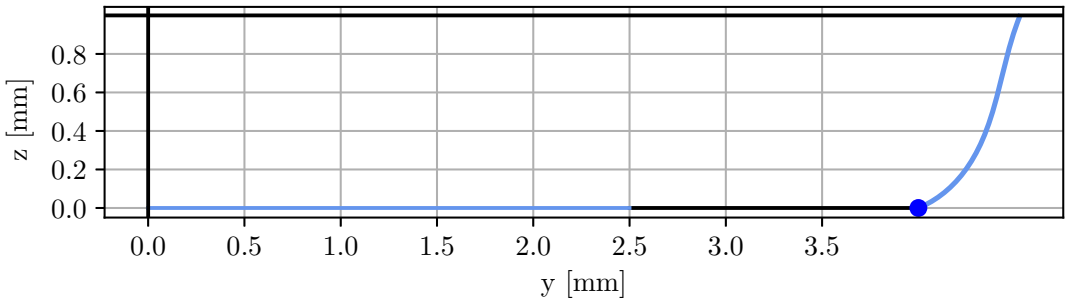

Figure 6.3: Shape of the interface water-air obtained from the numerical solution of the analytical problem constraint by the boundary set 3 and $H_{\text{up}} = 1$ mm. The top horizontal black line represents the top wall of the metering operation unit. The different parameters are $W_{\text{tot}} = 4$ mm, $t = 1$ mm, $g_{\text{art}} = 210$ m/s^2 and $\theta = 68$ °.

6.3.2 Computation of the H_{up} range

Now than shapes of interface attached to the top wall can be computed, a way to determine the limits $H_{\text{up,low}}$ and $H_{\text{up,high}}$ for a given θ must be established.

Firstly, $H_{\text{up,low}}$ is simply the maximum height of the interface attached to the left wall. Secondly, $H_{\text{up,high}}$ is determined in the same way as illustrated in Fig. 6.2. A range of increasing H_{up} is defined. The shape of the interface is computed as H_{up} increases. At a certain moment, the solver will begin to find two solutions for the same contact angle θ, one attached to the left wall and one to the top. In these cases, the total energies associated with both shapes are computed and the shape of minimal energy is determined. If the shape of minimal energy corresponds to the one attached to the top plane, H_{up} keeps increasing. On the other hand, if it corresponds to the shape attached on the left wall, the last H_{up} corresponds to the upper limit of the range.

6.4 Results

Now that a method to compute the range of H_{up} has been established, $H_{\text{up,low}}$ and $H_{\text{up,high}}$ can be computed for a range of contact angle θ.

Results showing the evolution of the upper and lower bound of the range for contact angles θ between 45° and 135° are obtained and are represented in Fig.6.4.

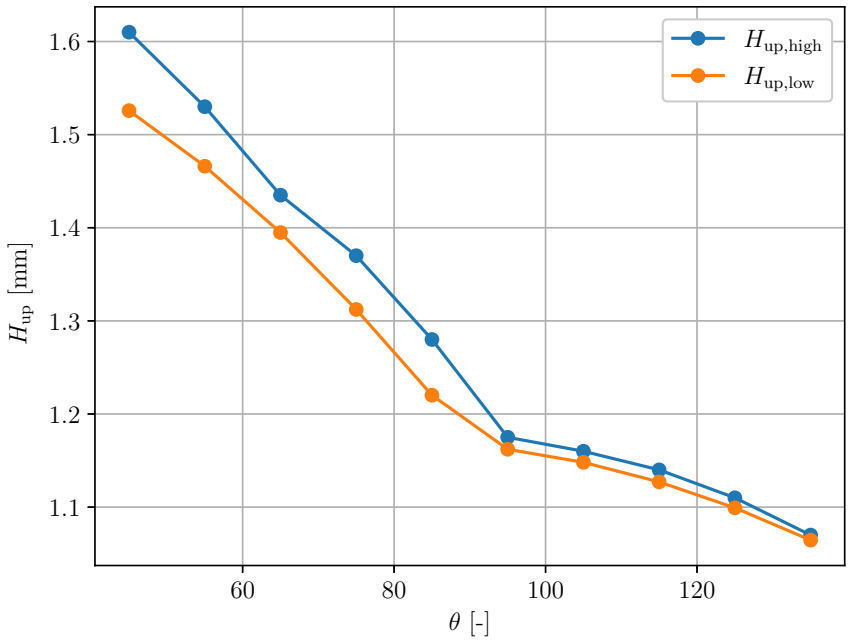

Figure 6.4: Evolution of the boundaries of the range of H_{up} where an attachment to the top wall is possible with respect to the contact angle θ. The parameters of the operation unit are $W_{\text{tot}} = 4$ mm, $t = 1$ mm, $g_{\text{art}} = 210$ m/s^2

6.4.1 Discussion

It can be seen in Fig. 6.4 that both limits of the range of H_{up} decrease as the contact angle increases. In fact, the meniscus is more and more flattened as the contact angle on the edge increases so it is not surprising that the different height of the top wall to which the liquid can attach itself decreases as θ increases.

Moreover, the experimenters could adapt the height of the top wall of the metering chamber according to the type of operation unit they want to build. Therefore, it is clear that the contact angle, and so the material used to fabricate the chip, must be taken into account during the design of the LoD.

However, it must be noticed that the difference between $H_{\text{up,low}}$ and $H_{\text{up,high}}$ is of the order of 0.1mm or less so that the range of H_{up} where two shapes of an interface can coexist and depend on the past of the system can nearly be negligible.

Finally, it must also be noticed that the range is smaller when $\theta > 90°$, i.e. for hydrophobic material. It can be concluded that for that type of material heights lying in a very narrow range correspond to the height where two possible shapes are possible.

CONCLUSION

In this thesis, an analytical model and a Surface Evolver model were developed to predict the liquid-air interface in a metering operation unit using a metering and a waste chamber. One model solves the system of ODEs describing the shape of the interface and the other model uses the Surface Evolver program. These two models were then used to study the sensitivity of the volume before the overflow, called critical volume, in the waste chamber with respect to different physical and geometrical parameters.

The first chapter introduced the theoretical basis in order to understand the physics in the metering chamber of the LoD. It also gave some information on the Surface Evolver program and the optimisation methods used.

In the second chapter, the exact geometry and physics problem have been defined. It has been concluded that the geometrical parameters influencing the volume selected by the operation unit were the distance W_{tot} [m] between the left wall and the inter-chamber right corner, the height H_{z} [m] of the triple line on the left wall, the thickness t [m] of the LoD and H_{up} [m] the distance between the inter-chamber horizontal plane and the top wall of the metering operation unit. Moreover, contact angle θ and the capillary length λ_{c} have been identified as the physical parameters that have an impact on the process. From those parameters, 4 dimensionless groups have been settled and are used in Chapter 5 in order to assess the sensitivity of the volume in the metering chamber to the different parameters. Finally, the quasi-static and local pinning-on-edge assumptions have been defined in order to model the problem numerically.

An analytical model was then introduced in Chapter 3. Its ability to predict the correct interface shape was demonstrated by comparing its results with those of the experiments carried out by the Microfluidic lab.

After that, a Surface Evolver model was presented in Chapter 4. This model was able to take into account the curvature of the interface in the depth of the LoD. It has been shown that the model is also able to predict correctly interface shapes. Moreover, the volume and energies obtained with both models have been compared and it has been concluded that both models

give similar results.

The fifth chapter presented the sensitivity analysis method based on both models as well as the results obtained . It has been concluded that there exists some proportionality between the volume and the dimensionless numbers and that the experimenters could adapt the selected volume by changing the rotational speed of the LoD. Moreover, it has been shown that the critical volume was the most sensitive to the artificial gravity and the depth of the metering chamber.

Finally, an analysis of the impact of the top wall of the metering chamber has been done in Chapter 6. It has shown that the meta-stable region of H_{up} where several shapes of interface could coexist was of the order of 0.1 mm and that the experimenters could adapt the material and height of the top wall depending on the type of operation unit they want to use.

Limitations and perspectives

The model and analysis produced in the scope of this thesis could be expanded in a number of ways:

- As mentioned in Ch. 2, the front wall of the metering operation unit is in fact made of hydrophobic tape. The SE model can simulate the hydrophobic wall, as shown in Fig. 6.5, but simulations could be performed in order to study the sensitivity of the critical volume with respect to a difference of contact angle between the front and back walls of the LoD.

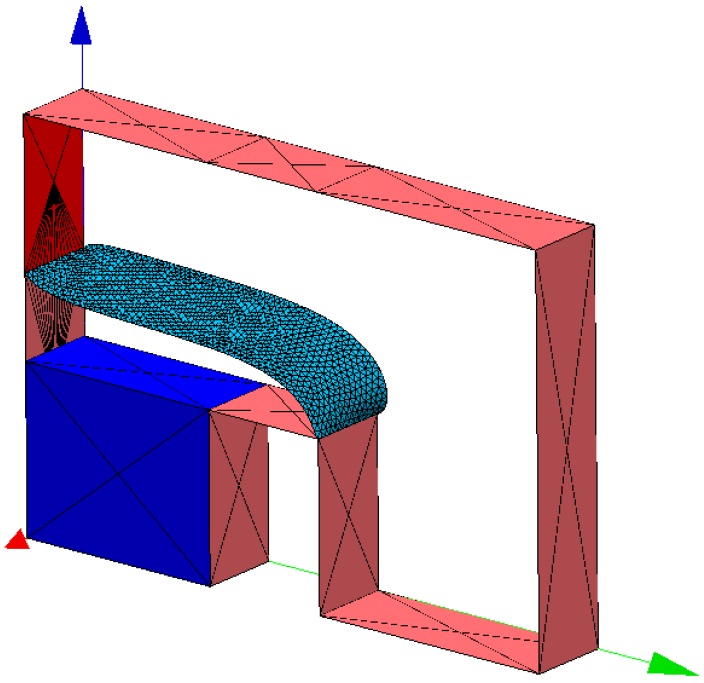

Figure 6.5: Shape of the interface for $V = 3.38$ mm and a hydrophobic front wall ($\theta_{\text{phob}} = 110°$, contact angle between the liquid and the hydrophobic tape). $W_{\text{tot}} = 4$ mm, $H_{\text{z}} = 1$ mm, $t = 1$ mm, $g_{\text{art}} = 210$ m/s^2 and $\theta = 65°$.

- The terrestrial gravity has been neglected during the whole study, even for low rotational

speed corresponding to $g_{\text{art}} = 50\,\text{m/s}^2$. A study taking into account the natural gravity and its relative effect on the shape of the interface at low rotational speed could be performed using the Surface Evolver model.

- The sensitivity of the critical volume has been studied on one specific geometry presenting a sharp edge at the inter-chamber. However many other geometry of the inter chamber can be explored. Here is a non-exhaustive list of possible other geometries to study with the Surface Evolver model: arched inter-chamber, saw-tooth-shaped inter-chamber, and steep inter-chamber.

- The impact of the attachment to the top wall has not been studied using Surface Evolver. The model developed in this thesis could be adapted in order to simulate this attachment in the program. Moreover, the meta-stable range of H_{up} has been studied for one set of parameters but could be explored with different sets.

APPENDIX A

SENSITIVITY ANALYSIS: SENSITIVITY COEFFICIENTS

H_z	π_1	g_{art}	π_2	$\theta = \pi_3$	S_{π_1}
mm	–	m/s^2	–	–	–
0.8	0.2	50	0.30	50	0.049
				65	0.003
				80	0
		200	0.15	50	0.104
				65	0.096
				80	0.069
		350	0.11	50	0.149
				65	0.12
				80	0.105
1.2	0.3	50	0.30	50	0.134
				65	0.114
				80	0.102
		200	0.15	50	0.164
				65	0.157
				80	0.152
		350	0.11	50	0.127
				65	0.128
				80	0.124
1.6	0.4	50	0.30	50	0.218
				65	0.197
				80	0.182
		200	0.15	50	0.149
				65	0.158
				80	0.167
		350	0.11	50	0
				65	0
				80	0

Table A.1: Sensitivity coefficient for each combination of parameters for a variation of $\pi_1 \pm 1\%$.

H_z	π_1	g_{art}	π_2	$\theta = \pi_3$	S_{π_2}
mm	–	m/s^2	–	–	–
0.8	0.2	50	0.30	50	0.681
				65	0.871
				80	0
		200	0.15	50	1.063
				65	1.206
				80	0.775
		350	0.11	50	0.811
				65	0.832
				80	0.860
1.2	0.3	50	0.30	50	0.646
				65	0.706
				80	0.765
		200	0.15	50	0.768
				65	0.806
				80	0.854
		350	0.11	50	0.862
				65	0.878
				80	0.883
1.6	0.4	50	0.30	50	0.617
				65	0.673
				80	0.726
		200	0.15	50	1.278
				65	1.006
				80	0.746
		350	0.11	50	0
				65	0
				80	0

Table A.2: Sensitivity coefficient for each combination of parameters for a variation of $\pi_2 \pm 1\%$.

H_z	π_1	g_{art}	π_2	$\theta = \pi_3$	S_{π_3}
mm	–	m/s^2	–	–	–
0.8	0.2	50	0.30	50	0.345
				65	0.378
				80	0
		200	0.15	50	0.211
				65	0.204
				80	0.170
		350	0.11	50	0.878
				65	0.187
				80	0.131
1.2	0.3	50	0.30	50	0.289
				65	0.308
				80	0.292
		200	0.15	50	0.197
				65	0.192
				80	0.156
		350	0.11	50	0.184
				65	0.043
				80	0.152
1.6	0.4	50	0.30	50	0.265
				65	0.288
				80	0.275
		200	0.15	50	0.191
				65	0.186
				80	0.152
		350	0.11	50	0
				65	0
				80	0

Table A.3: Sensitivity coefficient for each combination of parameters for a variation of $\pi_3 \pm 1\%$.

BIBLIOGRAPHY

[1] S. Hansen and A. Abd ElWahed. Point-of-care or point-of-need diagnostic tests: Time to change outbreak investigation and pathogen detection. *Tropical Medicine and Infectious Disease*, 5:151–166, (2020).

[2] R. Kraly, E. Holcomb, Q. Guana, and S. Henry. Review: Microfluidic applications in metabolomics and metabolic profiling. *Analytica Chimica Acta*, 653:23–25, (2009).

[3] J. Michael, T. Kim, V. Sunkara, and Y. Cho. Challenges and opportunities of centrifugal microfluidics for extreme point-of-care testing. *micromachines*, 7:32–46, (2016).

[4] R. Volpatti and K. Yetisen. Commercialization of microfluidic devices. *Trends in Biotechnology*, 32:347–350, (2014).

[5] O. Strohmeier, M. Keller, F. Schwemmer, S. Zehnle, D. Mark, F. von Stetten, R. Zengerleabc, and N. Paust. Centrifugal microfluidic platforms: advanced unit operations and applications. *The Royal Society of Chemistry*, 44:6187–6229, (2015).

[6] N. Israelachvili. *Intermolecular and surface forces*. Academic Press, (2011).

[7] J. Berthier and K. Brakke. *The physics of microdroplets*. J. Wiley, (2012).

[8] Y. Thomas. Iii. an essay on the cohesion of fluids. *Philosophical Transactions of the Royal Society of London*, 95:65–87, (1805).

[9] P-G. Gennes, F. Brochard-Wyart, and D. Quéré. *Capillarity and Wetting Phenomena: Drops, Bubbles, Pearls, Waves*. Springer New York, NY, (2004).

[10] K. Brakke. *Surface Evolver Manual*. Mathematics Department, Susquehanna University, (2013).

[11] K. Brakke. The surface evolver. *Experimental Mathematics*, 1, (1992).

[12] S. Ryaben'kii and V. Tsynkov. *A Theoretical Introduction to Numerical Analysis*. CRC Press, (2006).

[13] Y. Ma, X. Cao, X. Feng, Y., and H. Zou. Estimation of polymer/water interfacial tensions: hydrophobic homopolymer/water interfaces. *Polymer*, 48:7455–7460, (2007).